Detecting patterns of upwelling variability in Eastern Boundary Upwelling Systems with special emphasis on the Benguela region

Amieroh Abrahams

UNIVERSITY *of the* WESTERN CAPE

DEPARTMENT OF BIODIVERSITY & CONSERVATION BIOLOGY

A thesis submitted in fulfilment of the requirements for the degree of Magister Scientiae in the Department of Biodiversity and Conservation Biology, Faculty of Science, University of the Western Cape

Supervisor: Prof. A.J. Smit
Co supervisor: Dr. Robert Schlegel
September 2020

KEYWORDS

Code:R

In situ data

Ocean

Remotely-sensed data

Upwelling

Wind

ABSTRACT

Detecting patterns of upwelling variability in EBUS with special emphasis on the Benguela region

A. Abrahams

MSc. Thesis, Department of Biodiversity and Conservation Biology, University of the Western Cape.

Coastal upwelling is one of the most important oceanographic processes relating to ecosystem function at local and global spatial scales. To better understand how changes in upwelling trends may occur in the face of ongoing anthropogenically induced climate change it is important to quantify historical trends in climatic factors responsible for enabling coastal upwelling. However, a paucity of conclusive knowledge relating to patterns concerning changes in upwelling across the world's oceans over time makes such analyses difficult. In this study I aimed to quantify these patterns by first identifying when upwelling events occur using a novel method for predicting the behaviours of coastal upwelling systems over time. By using remotely sensed SST data of differing resolutions as well as several wind variables I was able to identify and quantify upwelling signals at several distances away from the coastline of various upwelling systems. Using this novel method of determining upwelling, I then compared upwelling patterns within all Eastern Boundary Upwelling Systems (EBUS) over a period of 37 years, with the assumption that climate change was likely to have driven variable wind patterns leading to a more intense upwelling over time. Overall, upwelling patterns and wind variables did not intensify overtime. This method of identifying upwelling may allow for the development of predictive capabilities to investigate upwelling trends in the future.

DECLARATION

I declare that "**Detecting patterns of upwelling variability in EBUS with special emphasis on the Benguela region**" is my own work, that it has not been submitted for any degree or examination at any university, and that all sources I have used or quoted have been indicated and acknowledged by complete references.

Full name: Amieroh Abrahams **Date:** 15 September 2020

Signature: .....…

ACKNOWLEDGEMENTS

I would like to acknowledge my supervisors. The support provided by them during this process were only surpassed by their insight into the methods allowing the production of this research. Additionally, I would also like to acknowledge all of the sources that contributed to the collection of the *in situ* coastal temperature data used in the second chapter of this thesis. I thank Jody Barends for assisting me throughout this project. This research was supported by the National Research Foundation Grant (SFH180604339745).

This Master's thesis covers the research I have performed over the last two years. This printed body of work is static in nature, the data science upon which it has been built is not. Much of this work may be found at my GitHub page: https://github.com/AmierohAbrahams/Upwelling_MCS.

TABLE OF CONTENTS

LIST OF FIGURES

LIST OF TABLES

CHAPTER 1

GENERAL INTRODUCTION

1.1. EBUSs and the Benguela upwelling system

Globally, there are four major Eastern Boundary Upwelling Systems (EBUS) distributed throughout western coastlines across the world's oceans. This includes the Benguela Current off south-western Africa; the Canary Current off north-western Africa, together with its northern extension off the Iberian Peninsula of south-western Europe; the Peru-Humboldt Current off western South America; and the California Current off the western continental USA and north-western Mexico (Bakun,1990; Pauly and Christensen, 1995; Bakun et al., 2015). Each of these systems are characterised as vast regions of coastal ocean that contain upwelled water located on the eastern side of their respective ocean basins. While these regions cover only 1% of the world's ocean surface, they are among the most productive regions of the ocean (Pauly and Christensen, 1995). This is due to these systems being subject to intensive coastal upwelling that brings cold, nutrient rich, high concentrated CO_2, low pH, and low oxygenated waters to the surface (Pauly and Christensen, 1995). As consequences of this upwelling, diverse marine fauna and flora are able to thrive in these areas due to the abundance of available nutrients.

The Benguela Upwelling System (BUS) is one of the most productive upwelling areas in the world ocean. The cold Benguela Current waters are bound in the south by the warm Agulhas retroflexion region and in the north by the southward flowing Angola Current. The Benguela system is split into northern (NBUS) and southern Benguela Upwelling Systems (SBUS) by a zone of intense perennial upwelling activity in Lüderitz within the Namibian region (Shannon, 1986; Cole, 1999). Meteorologically these regions are distinct. In the south, wind-induced upwelling reaches a maximum during spring and summer, whereas the northern region exhibits relatively less seasonal variation (Shannon, 1985). Coastal upwelling commonly occurs between Cape Agulhas, in the south, to souhern Angola in the north (Shannon 1985). The intensity of this upwelling is far from uniform, with spatio-temporal variability according to local bathymetry, fluctuations in the wind fields, coastally trapped waves and the intrusion of warm tropical waters from the northern and southern ends of the system (Shannon 1985). The flow of the Benguela Current is considered to be topographically guided (Nelson and Hutchings, 1983; Barange, 1991). The region surrounding the Benguela Current experiences a persistent alongshore wind which is associated with the St. Helena high pressure system (Guastella, 1992; Schultz, 2010). The continental shelf bathymetry and upwelling favourable winds provide a large-scale upwelling mechanism in the Benguela Current, whereas local bathygraphy and meteorology creates an alternating pattern of active and passive upwelling circulations along the coast (Chaigneau et al., 2009; Gutknecht et al., 2013). Upwelling occurring along the south coast of the Western Cape Province of South Africa, is generated by local winds which increase away from the coast (Fennel et al., 1999).

1.2. Upwelling

1.2.1. Atmospheric drivers of upwelling

EBUS forms part of the wind-driven ocean circulation. Their existence and dynamics are driven by wind direction and strength that cause Ekman transport that cannot be balanced by the horizontal advection of water (Bakun and Weeks, 2004; Capet et al., 2004). For nearly a century we have known that Ekman transport forced by equatorward upwelling-favourable winds is the main driver of the greatest eastern coastal upwelling systems (Sverdrup and Allen, 1939). During summer, when sea surface temperatures (SST) are warm, upwelling can be observed as a local temperature decrease (Gurova et al., 2013), with a typical time series of upwelling ranging from a few days to a few weeks. The wind responsible for coastal upwelling is dependent on pre-existing pressure gradients that respond to large-scale changes in global circulation like the location and intensity of subtropical anticyclones and associated trade winds, as well as to local processes associated with the establishment of thermal low pressure systems over the continents in the warm seasons (García-Reyes et al., 2015; Walker, 2020). Typically, upwelling favourable winds are caused by cross-shore atmospheric pressure gradients, and these gradients occur predominantly during heating periods.

Regions surrounding the Benguela EBUS, are dominated by anticyclonic high-pressure cells with quasi-stationary positions, resulting in abundant southerly and south easterly winds (Risien et al., 2004; Hagen et al., 2009). The South Atlantic Ocean High is situated along the west coast, drawing cool, dry air onto the west of the subcontinent (Van Heerden and Hurry, 1998). Solar heating during summer may result in the development of low-pressure cells known as heat lows which are absent during the winter (Tyson and Preston-Whyte, 2000). As the anticyclones shift north during winter months, the cold westerlies substantially impact on the weather of the

southern tip of the South African subcontinent (Van Heerden and Hurry, 1998). Further offshore, the wind stress curl causes upwelling by Ekman pumping. The coastal topography and the climatological winds frame the areas of upwelling (Shannon, 1985; Chavez and Messié, 2009).

1.2.2. Upwelling dynamics

The Humboldt Current is a highly productive, large marine ecosystem, where some of the largest fisheries of the world are located. Its productivity is dueto coastal upwelling that occurs all year round, especially along the coast of northern Chile and Peru (Blanco et al., 2001). Occassionaly the nutrient supply during upwelling is interrupted by influx of warm and nutrient-depleted equatorial waters (Montecino et al., 2005); during such events (El Niño, EN) the northward flow of cool nutrient-rich waters is suppressed and upwelling intensity is often reduced (Palma et al., 2006). The coastline of northern and central Chile is relatively straight, but in the nearshore region small-scale geographic features produce a high spatial heterogeneity, which also influences oceanographic conditions in this area. Several bay systemsare found along the coast of northern-central Chile. The the Canary Current, in its broadest sense, covers the latitudinal range 12–43°N, although both northern and southern limits shift seasonally. The Canary Current region is distinguished by its strong geographical diversity, which can determine the unique upwelling ecosystem response of different localities under similar annual and inter-annual forcing. The California Current system consists of a wind-driven surface current that flows southward along the coast. This current brings cool water from the Gulf of Alaska, which mixes with warmer tropical waters off the coast of southern California. One of the features of this system is the occurrence of wind-driven upwelling during the spring through fall seasons in the Northern region and to the Central region in all seasons. Heating of the land surface during the summer creates a thermal low pressure, while relatively high pressure remains in place over the cooler ocean surface. The Northern region is characterized by upwelling during the months of April through September. The onset of the upwelling is gradual, starting in March/April and ramping up to peak values in June/July. Termination of the upwelling season is rapid and typically occurs in October. In the Central region, upwelling occurs in all seasons. Upwelling intensity is greatest in the spring and summer months and diminishes in the fall and winter.

El Nino-Southern Oscillation (ENSO) is characterised by interannual SST variations. However, ENSO SST anomalies could also be derived from the central equatorial Pacific and spread toward the eastern Pacific (e.g., Wang 1995). This led to the suggestion that there may be more than one type of ENSO in the tropical Pacific, and the changes of the propagation direction may be a result of the alternation of different types of ENSO dynamics, such as the slow-SST type (Neelin 1991; Jin and Neelin 1993a,b) and the delayed-oscillator type (Schopf and Suarez 1988; Suarez and Schopf 1988; Battisti and Hirst 1989). ENSO events were usually classified according to their periodicity, propagation direction, onset time, or the associated zonal SST structure (e.g., Yasunari 1985; Fu et al. 1986; Barnett et al. 1991; Enfield and Cid 1991; Xu and Chan 2001). However, it appears that the shift of the SST anomaly centre between the eastern and central equatorial Pacific is a common contrasting feature among these various types of ENSO. During ENSO, the Trade winds are weakened or reversed, and as a result, central Pacific upwelling is turned into downwelling, creating a warm layer of SST (Klein et al., 1999; Wang and McPhaden, 2000; Beaufort et al., 2001). In general, regional ocean climate oscillations like the ENSO and Benguela Niño for the Benguela Current System show considerable variability in temperatures (Minobe et al., 1999) and complicated attempts to assess long term trends (Rimbu et al., 2003). However, many of the trends in recent decades might be associated with these oscillations (Barton et al., 2013). Some of these climate oscillations are expected to increase in amplitude or variance with climate change (Timmerman et al., 1999; Sydeman et al., 2013) which would further influence future upwelling trends.

EBUS have common properties (Blanco, 2001), where under typical conditions the main transport carries cold, well-oxygenated water from high towards low latitudes. The well-known Pacific El Niño (EN) manifest as an episodic warming of coastal waters off Peru. The ENSO caused marked changes in precipitation and wind patterns in the South-East Atlantic (Bakun, 1996; Shannon et al., 1996). The Humboldt Current (Peru-Chile) and California Current systems are both directly impacted from EN and La Niña (LN) (i.e. the warm and cold phases of the ENSO cycle) (Halpern, 2002; Arntz et al., 2006; Vargas et al., 2007). The Canary Current however is unique in that it does not have an oxygen minimum zone (OMZ) (Arístegui et al., 2009; Pelegrí and Peña-Izquierdo, 2015). OMZ is mainly affected by warm and cold phases of the ENSO. During EN, intra-seasonal Equatorial Kelvin Waves (IEKW) are generated by wind anomalies in the Equatorial Pacific region (Kessler et al., 1995). They propagate eastward and reach the western coasts of the Americas (Gushchina et al., 2012). There, they trigger coastal trapped waves (CTWs) which propagate poleward and impact the vertical structure of physical and biogeochemical variables alongshore off Peru (Echevin et al., 2014; Graco et al., 2017) and Chile

(Ulloa et al., 2001). The water column thus becomes oxygenated during EN and a deeper oxycline (>100 m) is observed, while during LN (e.g., 1999–2000), a shallower oxycline is described (Morales et al., 1999). Coastal upwelling within the Humboldt current exhibits strong interannual variability forced by the ENSO cycle, especially to its warm phase EN (Escribano et al., 2004). Oceanographic changes included the intrusion of oceanic, low-nutrient, and highly oxygenated waters into the coastal areas, with positive SST anomalies. Three main features are present under EN conditions, (i) raise in sea surface temperature, (ii) change of water mass distribution toward the coast, and (iii) decrease of primary production. Although upwelling-favourable winds can increase during EN and the depth of the upwelling source waters can remain unaffected, the nutrient supply to surface waters often decreases as the result of physical processes that involve downwelling and offshore transport, consequently primary production is reduced under such scenarios (Espinoza-Morriberon et al., 2017). The main physical processes connecting ENSO with the northern upwelling region are related to thermocline perturbations and changes in the alongshore currents forced by equatorial Kelvin waves (Shaffer et al., 1997).

The Benguela region expresses the Benguela Niños and are less frequent and intense than the Pacific events (Cury and Shannon, 2004; Florenchie et al., 2004). Benguela Niños are defined as anomalous warm events occurring between the southward flowing Angola Current and the BUS off south western Africa (Shannon, 1986). The annual southward migration of the Angola Benguela front introduces warm, saline Angolan water into Namibian coastal water. This seasonal migration is associated with the relaxation of the equatorward, upwelling-favourable wind stress (Boyd et al., 1987), while the southward penetration of warm saline water during the Benguela Niño does not seem to be associated with local winds (Stander and De Decker, 1969). Evidently, Benguela Niños are expressed as regions of abnormal, persistent high SST. Many researchers often associate the equatorial interannual variability pattern in the Atlantic to the ENSO phenomenon (Zebiak, 1993; Sutton et al., 2000). Servain (1985) suggested that eastern tropic oceans are governed by remote wind stress effects through equatorial wave dynamics. The Benguela Niño is believed to be associated with large-scale remote changes in the wind patterns. Hence, anomalies in trade winds may result in Kelvin waves that propagate eastward along the equator, inducing a deepening or a lifting of the thermocline. These warm events are also known to impact fisheries and the climate of this region and are also proven to induce unexpected rainfall events and drastically influence fish abundance and distribution (Boyer and Hampton, 2001; Rouault et al., 2003).

1.2.3. Trends

Research examining the trends in upwelling favourable winds have found variable results. This is due to small amplitude of uni-directional wind trends relative to amplitudes of seasonal and decadal wind variability, the short duration of time series relative to decadal variability, inconsistencies in data treatment and changes in measurement techniques used to interpolate or reanalyse data (Cardone et al., 1990). Sydeman et al. (2014) found a more accurate pattern of intensifying upwelling favourable winds in the Humboldt and California systems. In the Canary Current however, upwelling favourable winds tend to weaken in some regions. Importantly, there is a strong agreement that significant trends in upwelling intensifications are evident at higher latitudes for all EBUS (Alves. and Miranda, 2013; Barton et al., 2013; Stocker et al., 2013). Of all EBUS, the most information on this subject is available from the California Current. In the central-northern portion of this system, upwelling winds primarily occur during the warm months of the year, while the seasonal range of pressure gradients in the southern portion of the system is reduced, and upwelling can occur there year-round. Overtime, the timing of upwelling has trended toward later and shorter upwelling seasons in the northern portion of the California system and longer upwelling seasons in the southern portion (Bograd et al., 2009). In contrast, a modelling study on wind stress curl found increased upwelling in the late season in the northern California system (Diffenbaugh et al., 2004).

The changes in trends derived from models may be due to their coarse resolution, which does not adequately represent smaller scale coastal processes such as upwelling (Caabella et al., 2014). Alternatively, this might be due to failing to adequately incorporate factors such as cloud cover or land-ocean pressure gradients which are useful to identify upwelling. Downscaling global models to the coastal domain of EBUS is required to address some of these issues. When incorporating these factors in studies, promising results are obtained (Garreaud and Falvey, 2009).

There is substantial but conflicting evidence on SST trends in EBUS (Rimbu et al., 2003; Belkin, 2009; Garcia-Reyes and Largier 2010). This is because spatio-temporal resolutions of SST capturing various aspects of upwelling processes and trends are unclear by the interannual to multi-decadal variability that result from oceanographic and atmospheric processes (Snyder et al., 2003). Different SST of differing resolutions suggest

different trends within EBUS (Rimbu et al., 2003). The coarse resolution of SST datasets often makes it extremely difficult to separate nearshore upwelling related temperatures from regional and EBUS temperatures. These data products are also unable to solve small scale advection or retention within these systems which ultimately show different trends. Lima and Wethey (2012) use high resolution data to show cooling trends for coastal areas in all but the Canary upwelling system. A consistent agreement among all research of EBUS is that coastal and offshore temperature trends differ. These studies show increasing or decreasing trends in the nearshore SST, compared with increasing trends in the Benguela (Rouault et al., 2010; Santos et al., 2012) and California upwelling systems (Mote and Salathé, 2010). These trends match the trends of increasing upwelling favourable winds (Sydeman et al., 2014). Climate change associated trends in EBUS may be uncertain due to the effects of inshore cooling and offshore warming.

The Humboldt Current system is found to be the only EBUS whose SST trends shows a consistent negative linear trend over a time series of 36 years (Baumann and Doherty, 2013; Seabra et al., 2019). The Aguirre et al. (2019) reanalysis of an ensemble of GCMs found increases in summertime upwelling-favourable winds for both the Benguela Current system (BCS) and Canary Current system (CnCS). For the CnCS, Rykaczewski et al. (2015) found that a majority of models project significant increases in summertime intensity of upwelling; however, both Wang et al. (2015) and Rykaczewski et al. (2015) detected weakening in upwelling for the lowest latitudes of the CnCS.

1.2.4. Climate Change

Climate change as a result of anthropogenic warming is a global concern of both scientific and political importance. As the human population grows, the rate of global warming increases, resulting in profound effects on marine and other ecosystems (Stenseth et al., 2002; Harley et al., 2006; Hoegh-Guldberg and Bruno, 2010). Increasing temperatures cause a host of additional changes to marine systems, such as rising sea levels, increased ocean stratification, decreased sea-ice extent, and altered patterns of ocean circulation and precipitation (Doney et al., 2011). As this warming intensifies, pressure gradients between land and sea increases, resulting in a greater intensity of upwelling winds (Bakun, 1990; 2010; 2015). In rare cases, projected upwelling increases may overcome the countervailing effects of upper-ocean warming and stratification to cause regional cooling (Auad et al., 2006). Mead et al. (2013) found that coastal ecosystems are at high risk as a result of climate change. More recently, Whitfield et al. (2016) confirmed that coastal biodiversity has been observed to be affected by these effects.

While EBUS have long been on the minds of researchers, their reaction to climate change was not completely questioned until 1990 when Andrew Bakun, published his seemingly simple, yet polemic hypothesis (Sydeman et al., 2014; Bakun et al., 2015). Although Bakun (1990) did not explicitly conclude that the primary productivity of these regions will increase with climate change, it is well understood that the livelihood of pelagic fish is linked to upwelling trends; therefore, in addition to predicting an increase in the rate of upwelling, the Bakun Hypothesis has been extended to postulations that envisage direct benefits for EBUS fisheries (Bakun, 2015).

1.2.5. The Bakun Hypothesis

The atmospheric and oceanic mechanisms responsible for upwelling are interdependent and a change in one variable such as wind direction can have an effect on the distantly related variables. Over the past three decades, the earth's atmospheric temperature has warmed by 1.2°C (Wycech et al., 2020) and the earth’s oceans have warmed by approximately 0.6°C (Levitus et al., 2001). Although both land and sea surface temperatures are expected to increase, the land's lower heat capacity will cause it to warm more rapidly than the earth’s ocean (Huyer, 1983; Samantha et al., 2019; Zhang et al., 2019; Jakoboski et al., 2020). These differing heat capacities have led to an overall increase in the pressure gradient force occurring between land and sea. Implications of the pressure gradient force directly increase the equatorial wind speeds. As wind speeds accelerate, the rate of Ekman transport increases resulting in a larger amount of surface waters transferred offshore (Huyer, 1983). When coastal surface waters are displaced faster, the rate of coastal upwelling increases (Bakun et al., 2015). Given this, Bakun et al. (2010) proposed that if there was an increase in greenhouse gases, it would cause more heating during the day and more cooling during the night causing the temperature gradient to increase resulting in a strong pressure gradient, ultimately affecting wind patterns and therefore upwelling, imposing uncertainty in future upwelling trends (Bakun et al., 1990).

The hypothesis remains debated throughout the oceanographic community. Some researchers deny the logic behind this hypothesis and claim that EBUS warm faster than their neighbouring oceans, thus intensifying pre-existing land-sea pressure gradients. However, researchers also question whether the impact of differential heating has on pressure gradient force ultimately drives the intensification of upwelling within these regions (Rykaczewski et al., 2015; Brady et al., 2017). Rykaczewski et al. (2015) suggests that the mechanisms responsible for the intensification of upwelling dependent pressure gradient force is not driven by differential warming but rather intensifications are constrained to the poleward boundaries of the system and its upwelling season (Morgan et al., 2003; Biller et al., 2013; Rollo et al., 2020).

1.3. Extreme events in the context of upwelling

Extreme events such as marine heatwaves as defined by Hobday et al. (2016) are prolonged discrete anomalously warm water events that can be described by various statistical metrics such as intensity, duration and the count of events within a time series irrespective of its geographical location. Schlegel and Smit (2018) developed an algorithm that detects extreme events within long-term (> 30 years) daily time series of SST. It does so by finding the occasions when SST exceeds a threshold (the 90th percentile) in the probability distribution of the data based on an 11-day wide moving mean smoother centred on each day-of-the-year at each pixel. Similarly, upwelling signals could be detected in the same way by identifying a threshold when drops in temperature occur and by considering wind patterns as well as duration in order to classify an upwelling signal. Metrics of these upwelling signals could then be compared over a long time series to test for upwelling trends.

1.4. Rationale

Coastal upwelling impacts local climates and ecosystems by lowering atmospheric surface temperatures and thus influencing wind patterns. While the width of upwelling bands only extends 10-30 km, their productive band extends to approximately 100 km. Hence, coastal upwelling serves as a host of nutrients for phytoplankton (Send et al., 1987), creating a region of survival and prosperity for small pelagic fish (Carr, 2001). Given the importance of coastal upwelling; understanding upwelling trends over time and finding an accurate way of identifying upwelling signals are important. By using the extreme event algorithm, we were able to identify signals to date, duration and intensity.

Since EBUS are responsible for over 17% of global fish catch, their response to climate change has become of particular interest to oceanographers and climatologists (Carr, 2001). During summer months, coastal winds are strengthened by the land based thermal low-pressure system, generally located east of permanent but seasonally migrating oceanic high pressure systems (Huyer, 1983; Seager et al., 2003; Montecino and Lange, 2009). The biological productivity in EBUS being mainly as a result of warm seasonal upwelling, this study is important to test for variation in the duration, frequency and intensity of upwelling specifically during summer months.

1.4.1. Predictions/Hypotheses

We predict that intensified upwelling-favourable winds would lead to an increased upwelling rate and duration of these signals. Increased upwelling rates have significant effects on the surrounding ecosystems and fisheries (Bakun 1990, Bakun et al., 2010). As such, it is important to monitor upwelling trends during the most predominant upwelling period. The importance of coastal upwelling systems is widely recognised but their behaviour is still uncertain (Bakun et al., 2010). Here we hypothesize that upwelling detected at the coastline (0 km) are not the same signal detected at a distance of 50 km from the coastline given the differences in resolution of SST remotely sensed data. It is also predicted that a higher resolution SST data would detect an upwelling signal compared to coarse resolution data. It may therefore be assumed that human responses to poor upwelling detections and changes in upwelling trends as a result of climate change will negatively influence these productive zones. In order to investigate upwelling trends, the detection and collection of SSTs, wind speed, and wind direction data are important. The method used to detect upwelling will represent an extensive body of work and so the application of these results to biotic factors will not be accomplished extensively in this thesis. The important knowledge obtained by this research will branch out into different fields of study, with this it is critical that the work done within this thesis is accessible to other research groups.

CHAPTER 2

UPWELLING SIGNALS: A COMPARISON OF SEA SURFACE TEMPERATURE IN THE BENGUELA

Abstract

The importance of coastal upwelling systems is widely recognised. However, several aspects of the current and future behaviours of these systems remain uncertain. Fluctuations in temperature as a consequence of anthropogenic climate change are hypothesised to affect upwelling-favourable winds and coastal upwelling is expected to intensify across all Eastern Boundary Upwelling Systems. In this chapter we used sea surface temperature data from five different products of varying resolutions, in conjunction with wind data, to detect and analyse upwelling signals at four sites within the Benguela Upwelling System at varying distances from the coastline. We found that upwelling signals were not uniformly detected across the five products for each of the four sites and that the durations of those signals were longer when using SST data products with higher spatial resolutions. Moreover, the high-resolution data products were significantly more likely to display upwelling signals at a distance of 25 km away from the coastline when signals were also detected at the shoreline. Our findings promote the viability of SST and wind time series data towards detecting and predicting upwelling signals within coastal upwelling systems. However, our results also highlight the importance of high-resolution data products to improve the accuracy of such estimates. This study represents an important step towards the development of a novel method for predicting the behaviours of coastal upwelling systems.

Keywords: Seawater temperature, coastal regions, code: R, upwelling

2.1. Introduction

Sea surface temperature (SST) is regarded as one of the most important variables in the coupled ocean-atmosphere systems, and is a particularly useful research tool in the scientific fields of meteorology and oceanography (Mesias et al., 2007; Harlass et al., 2015). For over 150 years, SST data have been collected using *in situ* measurement techniques (Rayner et al., 2003) with satellite measurements of SST being available since the 1970s (Reynolds et al., 2013). Over the past decade, techniques have been developed to allow the assimilation and blending of different SST datasets from various *in situ* and satellite platforms. These are referred to as the Level-3 and Level-4 high resolution gap-free products. Previous studies demonstrated that satellite-based SST data are less accurate than *in situ* data due to the complexity of the oceanic and atmospheric conditions that need to be accounted for in deriving satellite SST products (Robinson et al., 1984; Brown et al., 1985; Minnett, 1991; Smit et al., 2013). The reason for this is that the sensors only 'look' at a restricted portion of the ocean for several minutes at a time; the exception being of-course, geo-stationary satellites like the POES (polar orbiting environmental satellite). These errors vary both regionally and temporally (Wick et al., 1992). In comparison to *in situ* SST measurements collected from ships or buoys, a major advantage of satellite SST is their global coverage and near real time availability. SST datasets with a high level of accuracy, spatial completeness, and fine-scale resolution are necessary for weather and climate forecasting and are of great importance for reliable climate change monitoring (Reynolds and Smith, 1995; Smith et al., 1998; Reynolds and Smith, 2002; Chao et al., 2009).

Long-term SST data have been obtained from two kinds of satellite remote sensors. Thermal infrared (TIR) and microwave (MW) sensors have different weather sensitivity characteristics and accuracies (Li et al., 2013). TIR SST products are available from the 1970s and may have a spatial resolution as fine as approximately a 4 km grid; however, they are affected by the presence of clouds and other aerosols in the atmosphere, which is known to result in spatial discontinuity. MW SST products have a lower resolution than TIR SSTs at approximately a 25 km grid, leading to a much lower accuracy near coastlines (Parinussa et al., 2008; Li et al., 2013). By combining these different types of SST products, it is possible to take advantage of the strengths within both, and each sensor type can help produce an SST dataset with more spatial and temporal coverage and higher resolution.

For many applications, SST data are not used or provided at the full resolution of the sensors, but are averaged over defined areas in order to produce a gridded product (Reynolds et al., 2002; Bulgin et al., 2016). Gridding in this way destroys more detailed information and as a result a gridded SST measurement is taken as an estimate of the average SST across a specific grid cell over a certain time period. Spatial sampling uncertainty and temporal averaging is present in gridded products as the full gridded cell is often not being observed as a result of interference due to the presence of clouds or aerosols, as previously mentioned. In existing daily global SST analysis products, typical grid resolution ranges from 0.05° × 0.05° to 0.25° × 0.25°, or from approximately 5 to 25 km (e.g., Reynolds and Smith, 1994; Brasnett, 2008; Donlon et al., 2012). Small-scale features can evolve during the course of the day, but the sensor sampling during this time is not dense enough for the sub-daily global analyses at a high spatial resolution (Reynolds and Chelton, 2010; Reynolds et al., 2013). Furthermore, considering that the satellites are passing overhead only once every ~24 hours, images are only captured at very specific times during the day. To capture these small-scale features in a gridded analysis, it is suggested that the development of an improved analysis would have high resolution at small-scale features in regions of good coverage and lower resolution in areas of poor coverage (Reynolds et al., 2013).

In order to assess the suitability of a range of SST products for the detection of upwelling signals, this study aimed to observe patterns and trends in upwelling signals in the Benguela upwelling system (BUS) across a range of localities and spatial scales off the South African West Coast specifically the Southern Benguela Upwelling System (SBUS). We selected an upwelling system for this study because this physical process provides a strong signal of increasing and decreasing SST that is strongly localised to known centres of upwelling, and which relates to the coastal wind field that drives the offshore advection of water mass. Here, a unique method for identifying upwelling signals was used. This method made use of wind variables as seen in Fielding and Davis (1989), but also applied a novel upwelling signal detection method to SST, which allowed for a more accurate identification of upwelling. Because upwelling is such a well characterised oceanographic process, the resultant fluctuating SST signal should be observed across independent SST products. Here we assess blended SST products covering a range of spatial grid resolutions from 0.05° × 0.05° to 0.25° × 0.25°.

The The SACTN dataset was the primary source of data used in this study to identify upwelling sites. This dataset consisted of coastal seawater temperatures for 129 sites along the coast of South Africa, measured daily from 1972 until 2017. We hypothesised that the higher resolution data should have a better fidelity at detecting these upwelling signals, some of which might only be confined to smaller spatial scales or localised closer to the shore.

The BUS is one of the four major Eastern Boundary Upwelling Systems (EBUS) (Bakun et al., 2015). EBUS are characterised as vast regions of coastal ocean occurring along the western shores of continents bordering the Pacific and Atlantic Oceans (Bakun, 1990; Pauly and Christensen, 1995; Bakun et al., 2010; Bakun et al., 2015). Coastal upwelling associated with EBUS is known to have a large influence on the associated ecosystem's primary productivity, and hence the abundance, diversity, distribution and production of marine organisms at all trophic levels (Bakun et al., 2010; 2015). The upwelling process is also hypothesised to be strongly affected by anthropogenic climate change. According to the 'Bakun hypothesis,' an increase in greenhouse gases will result in an increase in day-time warming and night-time cooling and ultimately cause an increase in temperature gradients which will form stronger atmospheric pressure gradients (Bakun, 1990). These pressure gradients modulate the winds which ultimately affect the intensity and duration of upwelling (Hsieh and Boer, 1992; Mote and Mantua, 2002; Bakun et al., 2010; Lima and Wethey, 2012). Concrete evidence in support of Bakun's hypothesis is not yet available (see Chapter 3)—I believe because of the difficulties associated with identifying the upwelling signals themselves. I anticipate that the work outlined in this chapter will make a valuable contribution in this regard, and to this this end I will apply the learning emerging here to Chapter 3, where trends in upwelling dynamics will be assessed for the world's four major EBUS. Since changes in SST indirectly affect coastal communities, and have considerable, often far-reaching economic impacts (Murawski, 1993; Bakun et al., 2010), this work could be of great importance to our understanding of how climatic change might affect EBUS in decades to come.

2.2. Methods

2.2.1. Site Selection

The western region of the South African coastline is dominated by the Benguela Current, which forms the foundation of an Eastern Boundary Upwelling System (EBUS) (Hutchings et al., 2009), and it provides a natural laboratory for this study. Annual mean coastal seawater temperatures within this region is 12.3 ± 1.2°C at the western limit near the Namibian border. Seasonal upwelling is controlled by south-easterly trade winds, with intense upwelling occurring throughout the summer months. This creates distinct temperature variations with much lower temperatures within the upwelling cells over a fairly narrow continental shelf found from the Cape Peninsula to Cape Columbine. In order to examine upwelling patterns at different distances from the coastline within the southern Benguela region, several sites from the SACTN dataset (Schlegel and Smit, 2016; Schlegel et al., 2017) along the west coast of South Africa were selected. The main objective of this study was to identify upwelling signals with a variety of data products. This involved four separate SST products that covered a time period of four years. To assess upwelling metrics within the BUS, four sites were selected as points of comparison. Each site was situated along the West Coast of South Africa at various distances from the upwelling centre of the BUS (**Figure 2.1**).

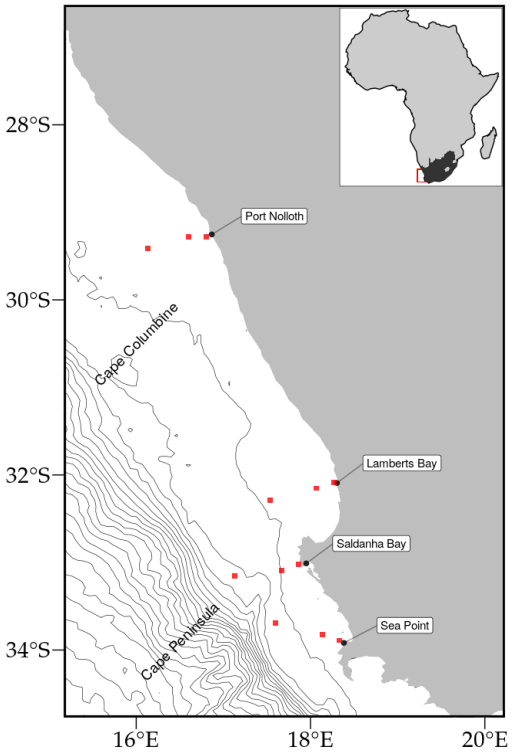

Figure 2.1: Map of southern Africa showing the coastal bathymetry. The black points represent the location of the in situ temperature sites and the empty red boxes show the pixels used along the shore normal transect from the satellite sea surface temperatures (SST) time series. The red boxes are at 0 km, 25 km and 50 km from the coastline.

2.2.2 Datasets

This study uses four Level-4 remotely sensed temperature datasets compiled by a number of organisations. The AVHRR-only (Advanced Very High-Resolution Radiometer) Optimally-Interpolated Sea Surface Temperature (OISST) dataset has been providing global SSTs for nearly four decades (Reynolds and Smith, 1994). OISST is a global 0.25° × 0.25° gridded daily SST product that assimilates both remotely sensed and *in situ* sources of data to create a gap free product (Banzon et al., 2016). The version 3.0 Group for High Resolution Sea Surface Temperature (GHRSST) product has a 0.2° × 0.2° global grid resolution and is constructed by the Canadian Meteorological Center (CMC). It combines infrared satellite SST at numerous points in the time series from the AVHRR, the European Meteorological Operational-A (METOP-A) and Operational-B (METOP-B) platforms, as well as the microwave SST data from the Advanced Microwave Scanning Radiometer 2 in conjunction with *in situ* observations of SST from ships and buoys from the ICOADS program. The Multi-scale Ultra-high Resolution (MUR) SST Analysis is produced using satellite instruments with datasets spanning 1 June 2002 to present. MUR provides SST data at a spatial resolution of 0.01° × 0.01° and is currently among the highest resolution SST datasets available. The final dataset used is the GHRSST analysis produced daily using a multi-scale two-dimensional variational (MS-2DVAR) blending algorithm on a global 0.01° grid known as G1SST. This product uses satellite data from a variety of sensors, such as AVHRR, the Advanced Along Track Scanning Radiometer (AATSR), the Spinning Enhanced Visible and Infrared Imager (SEVIRI), the Moderate Resolution Imaging Spectroradiometer (MODIS), and *in situ* data from drifting and moored buoys. We see that not all products are completely independent as they share the use of AVHRR SST data, but the amount of subsequent blending, the incorporation of other SST data sources, the different blending and interpolation approaches used, and the differing final grid resolutions make them acceptably different for this study.

Additionally, this study uses the South African Coastal Temperature Network (SACTN) dataset for its *in situ* temperature records. This dataset consists of coastal seawater temperatures obtained from 129 sites along the South African coastline, measured daily from 1972 until 2017 (Schlegel and Smit, 2016; Schlegel et al., 2017). Of these, 80 were measured using hand-held thermometers and the remaining 45 were measured using underwater temperature recorders (UTRs). For this analysis, the data were combined and formatted into standardized comma separated values (CSV) files which allowed for a fixed methodology to be used across the entire dataset.

An advantage to using *in situ* data over satellite data is that they may provide a more accurate representation of the thermal properties closer to the coast, whereas satellite data often fail to accurately capture and represent temperature properties within the same spatial context. The result is that *in situ* data can more accurately explain upwelling signals within the coastal inshore environment. Further, evidence by Smit et al. (2013) has shown that satellite data along the South African coastline may have a warm bias as high as 6 °C greater than *in situ* temperatures within the nearshore environment. In order to create a time series of each of the remotely sensed SST data products, shore-normal transects of all Level-4 products were extended at west coast stations where the *in-situ* data in the SACTN database were available. Time series of SSTs were extracted at 0, 25 and 50 km along these shore-normal transects from the coast (**Figure 2.1**).

2.2.3 Wind data

Wind data were obtained from the South African Weather Service (SAWS), and were provided at three-hour resolutions. Specific wind characteristics were measured, namely, wind direction (dirw) and wind speed (spw). Wind was an important variable for this study as wind direction and wind speed have a direct influence on the intensity and duration of upwelling, consequently, wind data collected from 1989-01-01 to present were investigated for their relationship with upwelling at the sites for which SST time series were extracted.

2.2.4 Defining and determining upwelling

In order to detect and analyse upwelling signals at four sites within the BUS, it was first necessary to define when upwelling was occurring; however, to accomplish this a set of threshold values for identifying when the phenomenon was taking place was required. Given that upwelling is primarily caused by alongshore, equatorward winds, both SST and wind data were used. The wind data were used to inform an upwelling index calculated using the formula presented in the work by Fielding and Davis (1989):

$$upwelling\ index = \mu(\cos\theta - 160)$$

where μ represents the wind speed (m/s), θ represents the wind direction in degrees, and 160 is the orientation of the west coast (Jury 1980). The index relies heavily on wind speed and direction data in order to identify the presence and intensity of upwelling. The above equation produces a value called the upwelling index. An upwelling index < 0 represents downwelling whilst an upwelling index > 0 represents upwelling (Fielding and Davis, 1989). When the upwelling index is greater than 0, SSTs usually drop, as expected, suggesting that upwelling is occurring. Upwelling was found that the drop in SST that coincided with a positive upwelling index was close to the seasonally varying 25th percentile threshold for SST, so this threshold temperature was used in combination with the upwelling index to identify when upwelling may be occurring. With the threshold set for which temperatures may qualify as an upwelling signal it was then necessary to identify the number of consecutive days that must be exceeded for an upwelling signal to qualify as a discrete event. Here it must be noted that upwelling is known to vary on a seasonal basis and may also occur hourly (sub-daily). Therefore, the minimum duration for the classification of an upwelling signal was set as one day, the rationale being that data from the SACTN dataset as well as the satellite remotely sensed SST data are collected only at a daily resolution, preventing a temporally finer definition. With the upwelling index, temperature threshold, and duration for an upwelling signal established, the `detect_event()` function from the **heatwaveR** package (Schlegel and Smit, 2018) was used to calculate metrics for the upwelling signals. Because upwelling signals were calculated relative to percentile exceedances, rather than an absolute definition such as temperatures below a fixed temperature threshold, upwelling signals could occur any time of the year; however, upwelling was shown to be more dominant during summer months (December, January and February), as expected. This method of determining upwelling signals is unique as it considers both SST and wind pattern, and provides us with a descriptive statistical output of each of the signals detected (**Table 2.1**).

Table 2.1: Metrics of upwelling signals and their descriptions.

Name [unit]	Definition
Duration [days]	Consecutive period of time that temperature exceeds the threshold
Mean intensity [°C]	Highest temperature anomaly value during the signal
Cumulative intensity [°C.days]	Sum of the daily intensity anomalies over a duration of the event

ANOVAs were used to compare the upwelling metrics such as duration, intensity, and cumulative intensity against the main effects: *site*, *product* and *distance*. Upwelling metrics as a function of satellite product type was assessed using *product* as main effect, and nesting *distance* within *site*. To establish whether differences existed between sites or distances from the shore, the upwelling metrics were assessed as a function of *site* or *distance*, independently for each satellite. Restrictions to experimental design prevented testing interaction effects within *product* types. In the analysis the relationship between the SST products across the various selected study sites were established; factors used to correlate these relationships included duration and the number of signals detected. These analyses sought to test if significant differences occurred between sites and data products. A Pearson Product Moment correlation was used to identify if the same upwelling signal detected at a distance of 0 km from the coastline would be visible at a distance of 25 km from the coastline and similarly if the same upwelling signal could be observed when comparing at a distance of 0 and 50 km from the shore. The signals were classified by start and end date and within the same data product. Thereafter, the average numbers of upwelling signals detected by each individual data product across all sites were compared using an ANOVA test.

2.3. Results

A one-way ANOVA indicated no significant difference in upwelling duration between sites within the South African portion of the BUS as detected in the CMC (d.f. = 3, $F = 0.88$, $p > 0.05$) and OISST (d.f. = 3, $F = 0.76$, $p > 0.05$) (**Table 2.2**, **Figure 2.2**) products. However, a significant difference was found between the G1SST (d.f. = 3, $F = 3.46$, $p < 0.05$), MUR (d.f. = 3, $F = 4.45$, $p < 0.005$) and SACTN (d.f. = 3, $F = 3.61$, $p < 0.01$) data products. The Sea Point site had the longest mean duration of upwelling signals detected. Lamberts Bay and Port Nolloth had the shortest duration of upwelling signals detected. Particularly, Lamberts Bay in the SACTN data product yielded the shortest duration of upwelling signals.

A significant difference was found in upwelling mean intensity between sites in the CMC (d.f. = 3, $F = 5.29$, $p < 0.001$), OISST (d.f. = 3, $F = 7.56$, $p < 0.001$) and SACTN (d.f. = 3, $F = 17.82$, $p < 0.001$) products. However, no significant difference was found in the G1SST (d.f. = 3, $F = 2.01$, $p > 0.05$) and MUR (d.f. = 3, $F = 1.38$, $p < 0.05$) products (**Table 2.3**, **Figure 2.3**). Sea Point represents the highest mean intensity of upwelling signals collected among all of the remotely sensed SST. Differences in means were present across data products at each site individually but were consistent across sites (i.e. each data product detected a similar mean at each of the respective sites.

Table 2.2: One-way ANOVA evaluating the variation in the duration of upwelling signals detected in the various gridded SST and *in situ* products between four sites within the Benguela Current region of South Africa. Comparisons are graphically captured in **Figure 2.2**.

Data product		d.f.	M.S.	*F*-value	*P*-value
CMC	site	3	21.68	0.88	> 0.05
	residuals	132	24.52		
G1SST	site	3	158.99	3.46	< 0.05
	residuals	268	45.93		
MUR	site	3	445.1	4.45	< 0.005
	residuals	155	100.1		
OISST	site	3	68.13	0.76	> 0.05
	residuals	169	8895		
SACTN	site	3	24.84	3.61	< 0.01
	residuals	280	7.156		

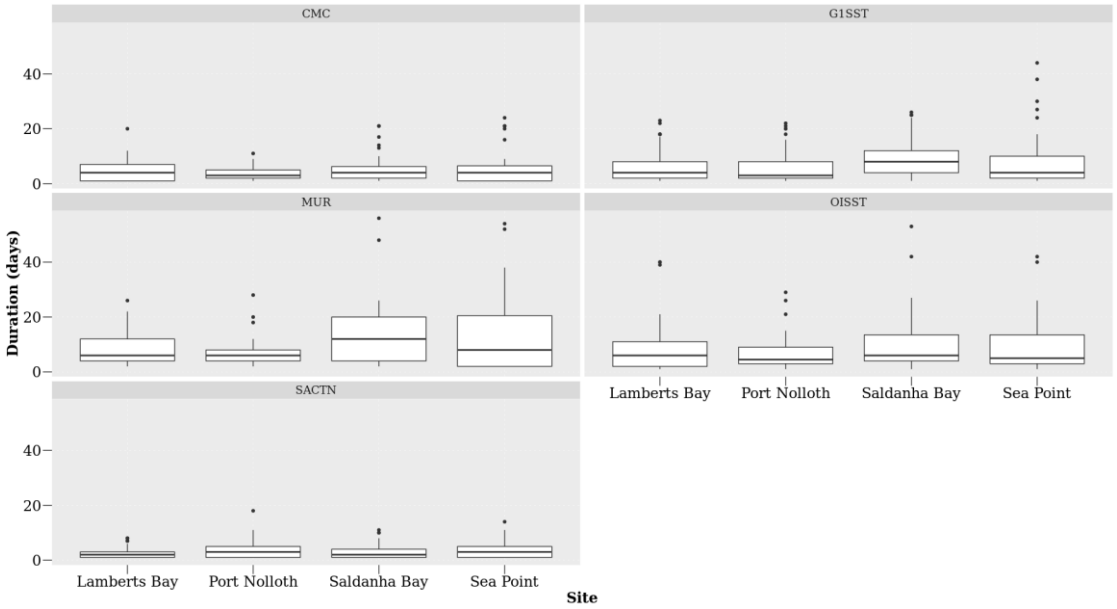

Figure 2.2: The upwelling duration for each of the signals detected for the four satellite products and the SACTN in situ collected data during summer months (December, January and February), over a four-year period.

Table 2.3: One-way ANOVA evaluating the variation in the mean intensity of upwelling signals detected in the four gridded SST and in situ products between the four sites within the Benguela Current region of South Africa. Comparisons are graphically captured in **Figure 2.3**.

Data product		**d.f.**	**M.S.**	***F*-value**	***P*-value**
CMC	site	3	0.56	5.29	< 0.001
	residuals	132	0.11		
G1SST	site	3	0.67	2.01	> 0.05
	residuals	268	0.34		
MUR	site	3	0.42	1.38	> 0.05
	residuals	155	0.31		
OISST	site	3	1.76	7.56	< 0.001
	residuals	168	0.23		
SACTN	site	3	5.29	17.82	< 0.001
	residuals	280	0.29		

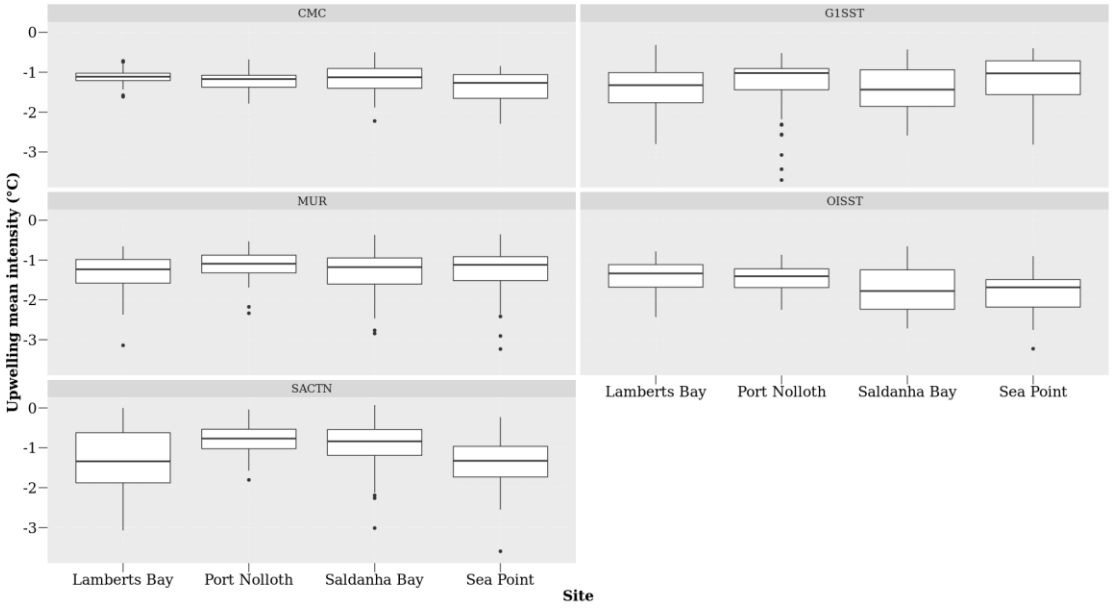

Figure 2.3: The mean intensity for each of the signals detected for the four satellite products and the SACTN in situ collected data during summer months (December, January and February), over a four-year period.

Table 2.4*:* One-way ANOVA evaluating the variation in upwelling cumulative intensity as detected in the four gridded SST and in situ products between four sites within the Benguela Current region of South Africa. Comparisons are graphically captured in **Figure 2.4**.

Data product		d.f.	M.S.	*F*-value	*P*-value
CMC	site	3	64.43	1.23	> 0.05
	residuals	132	52.25		
G1SST	site	3	500.9	2.96	< 0.05
	residuals	268	169.2		
MUR	site	3	2317.6	3.81	< 0.01
	residuals	155	609.5		
OISST	site	3	744.7	1.54	> 0.05
	residuals	169	484.8		
SACTN	site	3	122.53	9.44	< 0.0005
	residuals	280	12.98		

There was no significant difference in upwelling cumulative intensity between sites within the South African portion of the BUS as detected in the CMC (d.f. = 3, $F = 1.23$, $p = 0.3$) and OISST (d.f. = 3, $F = 1.54$, $p > 0.05$) data product (**Table 2.4**, **Figure 2.4**). A significant difference in cumulative intensity of upwelling signals was found in the G1SST (d.f. = 3, $F = 2.96$, $p < 0.05$), MUR (d.f. = 3, $F = 3.81$, $p < 0.01$) and SACTN (d.f. = 3, $F = 9.44$, $p < 0.001$) data products during the summer season. The cumulative intensity of upwelling signals was most intense in Saldanha Bay and Sea Point for the MUR, G1SST and OISST products. The cumulative intensity from sites within the SACTN data product were the lowest.

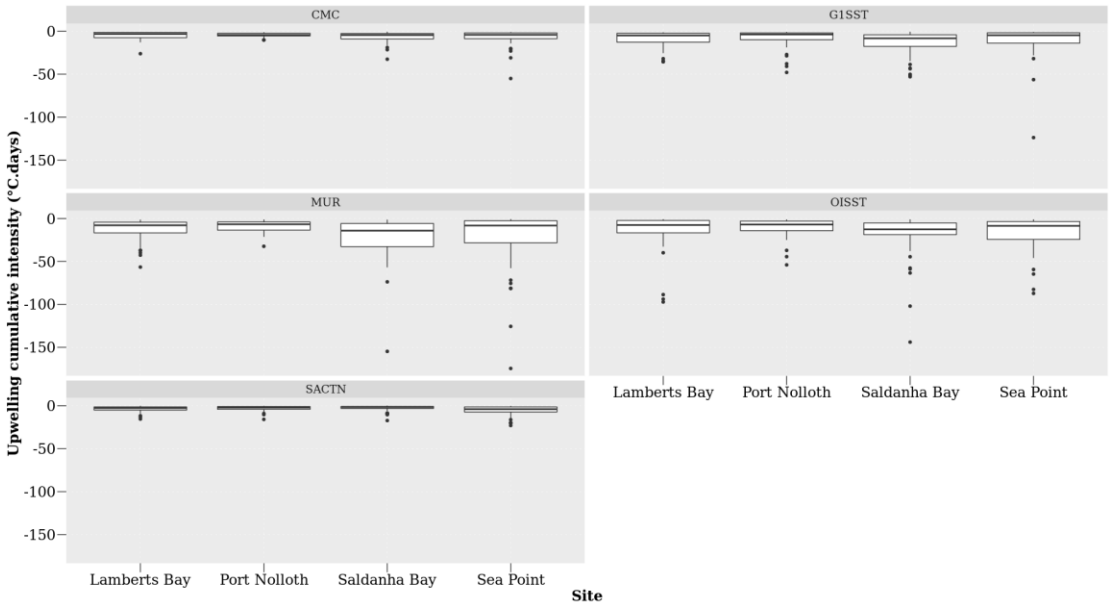

Figure 2.4: The upwelling cumulative intensity for each of the signals detected for the four satellite products and the SACTN in situ collected data during summer months (December, January and February), over a four-year period.

An ANOVA showed that no significant difference exist in the duration of upwelling signals detected at different distances from the shore during the summer season in the CMC (d.f. = 2, $F = 0.86$, $p > 0.04$), G1SST (d.f. = 2, $F = 0.59$, $p > 0.05$), MUR (d.f. = 2, $F = 2.29$, $p > 0.05$) and OISST data (d.f. = 2, $F = 1.61$, $p > 0.05$) products. The MUR and G1SST often detected the longest duration of upwelling signals at a distance of 0 and 25 km from the shore (**Table 2.5**, **Figure 2.5**).

Table 2.5: One-way ANOVA evaluating the variation in the duration of upwelling signals for the four gridded SST products between at the various distances from the shore. Comparisons are graphically captured in **Figure 2.5**.

Data product		**d.f.**	**M.S.**	***F*-value**	***P*-value**
CMC	distance	2	21.15	0.86	> 0.05
	residuals	133	24.5		
G1SST	distance	2	27.81	0.59	> 0.05
	residuals	269	47.33		
MUR	distance	2	308	2.29	> 0.05
	residuals	156	104.1		
OISST	distance	2	141.31	1.61	> 0.05
	residuals	170	87.89		

Table 2.6: One-way ANOVA evaluating the variation in the mean intensity of upwelling signals detected in the four gridded SST products from the shore. Comparisons are graphically captured in **Figure 2.6**.

Data product		d.f.	M.S.	*F*-value	*P*-value
CMC	distance	2	0.32	2.89	< 0.05
	residuals	133	0.11		
G1SST	distance	2	7.36	25.71	< 0.001
	residuals	269	0.25		
MUR	distance	2	5.29	21.74	< 0.0001
	residuals	156	0.24		
OISST	distance	2	1.62	6.68	< 0.001
	residuals	170	0.14		

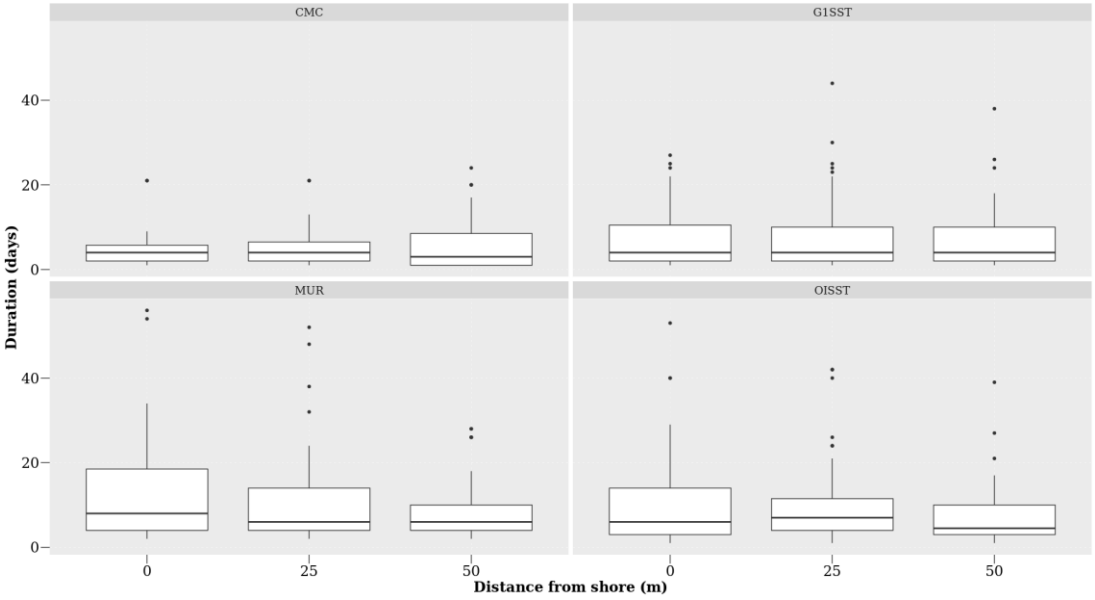

Figure 2.5: The duration for each of the signals detected at the various distances from the shore for the four satellite products during summer months (December, January and February), over a four-year period.

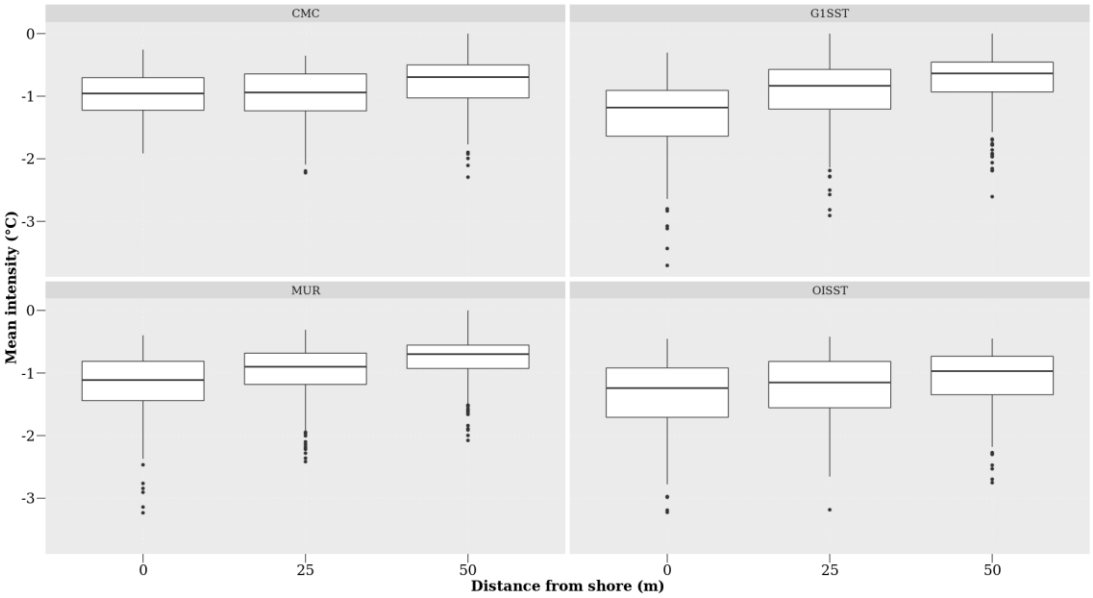

Figure 2.6: The mean intensity for each of the signals detected at the various distances from the shore for the four satellite products during summer months (December, January and February), over a four-year period.

Significant differences in the mean intensity of upwelling signals were detected at different distances in all of the remotely sensed SST products. CMC (d.f. = 2, F = 2.89, p < 0.05), G1SST (d.f. = 2, F = 25.71, p < 0.001), MUR (d.f = 2, F = 21.74, p < 0.001) and OISST (d.f. = 2, F = 6.68, p < 0.001). MUR and G1SST products recorded the highest mean intensity of upwelling signals at a distance of 0 km from the shore (**Table 2.6**, **Figure 2.6**). The mean intensity of upwelling decreased further away from the shore in all of the SST products.

Table 2.7: One-way ANOVA evaluating the variation in the cumulative intensity of upwelling signals detected in the four gridded SST products between at the various distances from the shore. Comparisons are graphically captured in **Figure 2.7**.

Data product		d.f.	M.S.	*F*-value	*P*-value
CMC	distance	2	48.62	0.93	> 0.05
	residuals	133	52.58		
G1SST	distance	2	915.1	5.47	< 0.05
	residuals	269	167.4		
MUR	distance	2	3860	6.42	< 0.05
	residuals	156	601		
OISST	distance	2	1061.3	2.19	> 0.05
	residuals	170	482.6		

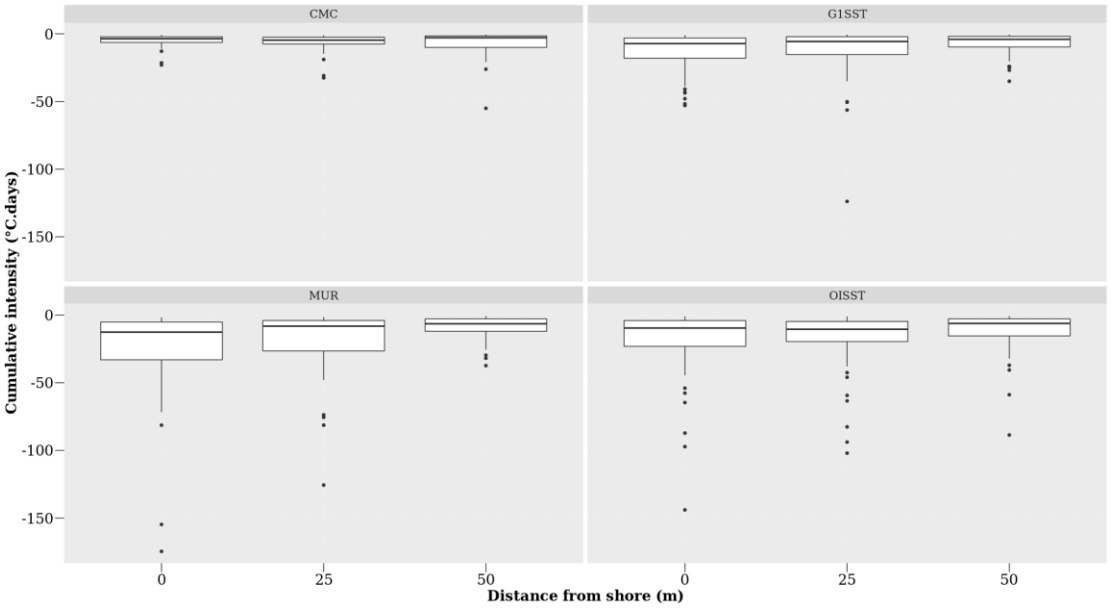

Figure 2.7: The cumulative intensity for each of the signals detected for the four satellite products during summer months (December, January and February), over a four-year period.

A one-way ANOVA showed a significant difference in the cumulative intensity of upwelling signals detected at different distances from the shore in the G1SST (d.f. = 2, $F = 5.46$, $p < 0.005$) and MUR (d.f. = 2, $F = 6.42$, $p < 0.005$) data products. (**Table 2.7**, **Figure 2.7**). However, the CMC (d.f. = 2, $F = 0.93$, $p > 0.05$) and OISST (d.f. = 2, $F = 2.19$, $p > 0.05$) products showed no significant difference in cumulative intensity of upwelling signals detected. The MUR and OISST product observed the highest cumulative intensity at a distance of 0 km from the coastline, this intensity decreased further away from the coastline. The cumulative intensity of upwelling signals for all product decreased further from the shore.

A nested ANOVA (**Table 2.8**, **Figure 2.8**) showed that there is a significant difference in the duration of upwelling signals detected amongst the data products (nested ANOVA, d.f. = 3, $F = 13.43$, $p < 0.001$). The MUR product had the longest duration of upwelling signals while the CMC products had the shortest.

Table 2.8: Nested ANOVA evaluating the variation in upwelling duration as detected in four gridded SST products (OISST, CMC, G1SST, and MUR) at several distances away from the shore and sites within the Benguela Current region of South Africa. Only the main effect due to 'product' is indicated. Comparisons are graphically captured in **Figure 2.8**.

	d.f.	**M.S.**	***F*-value**	***P-value***
Product	3	849.3	13.43	< 0.001
residuals	725	63.2		

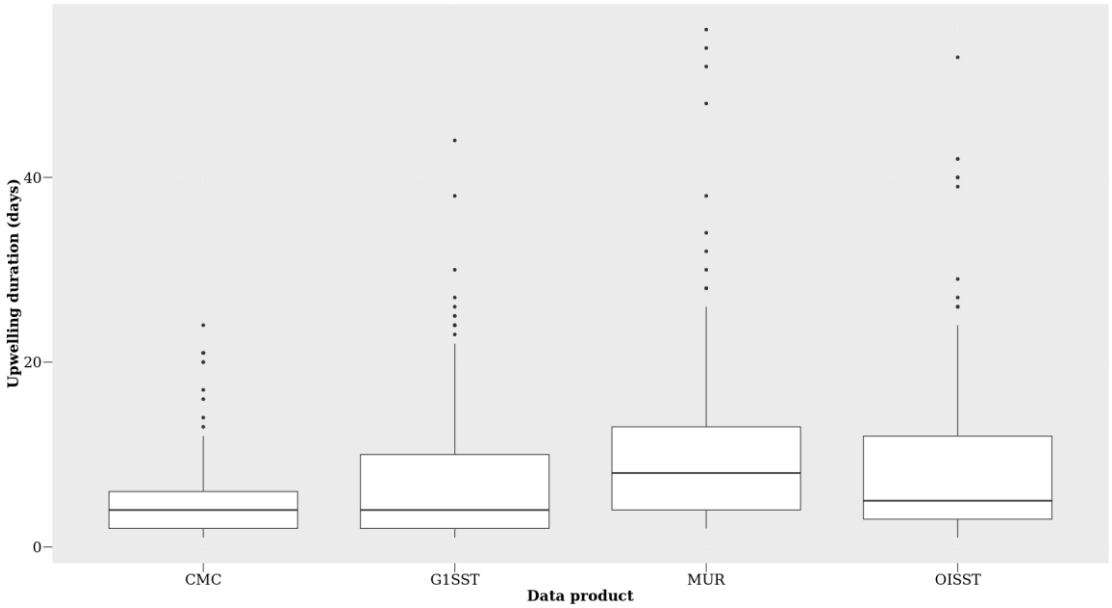

Figure 2.8: The duration of upwelling signals detected for the four satellite products at the different distances from the shore during summer months (December, January and February), over a four-year period.

Table 2.9: Nested ANOVA evaluating the variation in the mean intensity of upwelling signals detected in four gridded SST products (OISST, CMC, G1SST, and MUR) at several distances away from the shore and sites within the Benguela Current region of South Africa. Only the main effect due to 'product' is indicated. Comparisons are graphically captured in **Figure 2.9**.

	d.f.	**M.S.**	***F*-value**	***P-value***
Product	3	4.45	19.84	< 0.001
residuals	725	0.22		

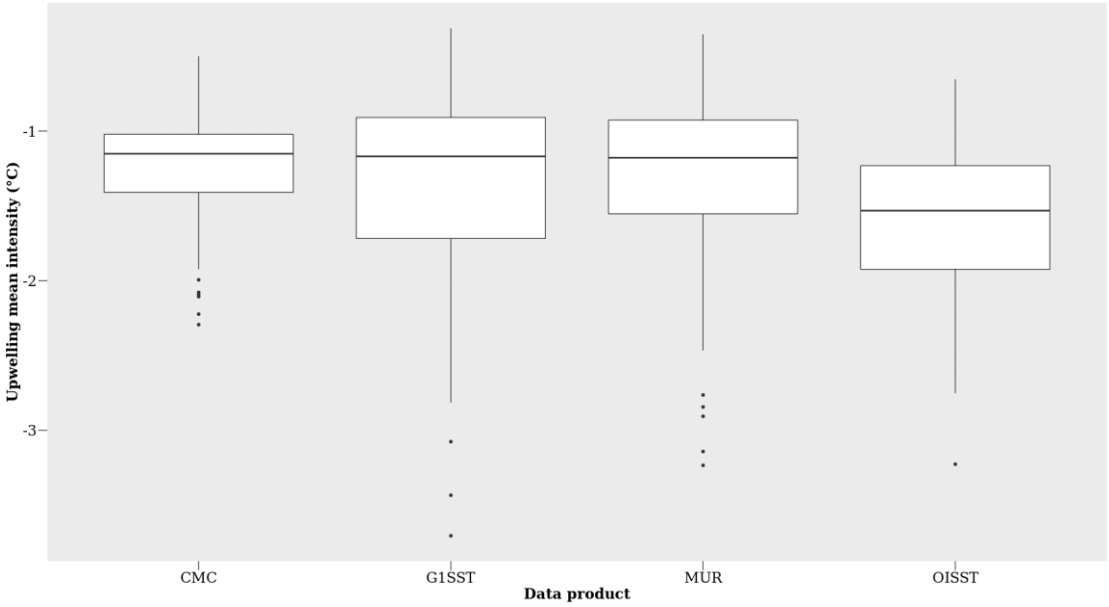

Figure 2.9: The mean intensity for each of the signals detected for the four satellite products at difference distances from the shore during summer months (December, January and February), over a four-year period.

The ANOVA analysis suggests (**Table 2.9**, **Figure 2.9**) that there is a significant difference in the mean intensity of upwelling signals detected between the data products of variable resolution (nested ANOVA, d.f. = 3, F = 19.84, $p < 0.001$). The G1SST and MUR data products represented the highest mean intensity while CMC represented the lowest mean intensity of upwelling signals.

There was a significant difference (**Table 2.10**, **Figure 2.10**) in the cumulative intensity of upwelling signals detected between the data products of variable resolution (nested ANOVA, d.f. = 3, F = 14.12, $p < 0.001$). The MUR SST product presented the highest cumulative intensity of upwelling signals and the CMC data represents the lowest cumulative intensity of upwelling signals detected.

Table 2.10: Nested ANOVA evaluating the variation in upwelling cumulative intensity as detected in four gridded SST products (OISST, CMC, G1SST, and MUR) at several distances away from the shore and sites within the Benguela Current region of South Africa. Only the main effect due to 'product' is indicated. Comparisons are graphically captured in **Figure 2.10**.

	d.f.	M.S.	*F*-value	*P-value*
Product	3	4306	14.12	< 0.001
residuals	725	305		

Pearson correlation analyses revealed that the possibility of observing the same upwelling signal detected at 0 km from the coast, at 25 km and at 50 km from the coast respectively varied across the individual data products at each of the four sites (**Table 2.11**). Overall, it was found that upwelling signals occurred simultaneously at 0 km and at 25 km considerably more frequently than between 0 km and 50 km from the coastline. In addition, the likelihood of detecting upwelling signals at 50 km from the coastline were notably lower throughout all pairwise comparisons, apart from signals detected at Port Nolloth, using the CMC, MUR, and G1SST products.

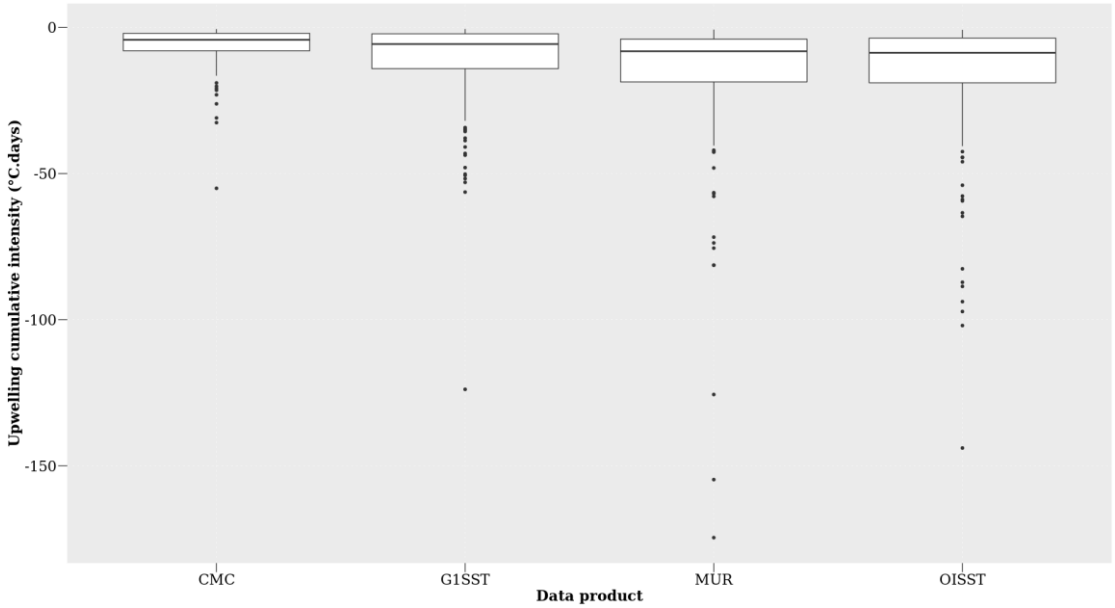

Figure 2.10: The cumulative intensity for each of the signals detected for the four satellite products at difference distances from the shore during summer months (December, January and February), over a four-year period.

Table 2.11: A Pearson correlation of the relationship between the number of signals detected at a distance of 0 km versus a distance of 25 km and between the number of signals at 0 km and 50 km.

Product	Site	0 km vs 25 km	0 km vs 50 km
OISST	Lamberts Bay	0.59	0.14
	Port Nolloth	0.76	0.38
	Saldanha Bay	0.65	0.42
	Sea Point	0.76	0.18
CMC	Lamberts Bay	0.12	0.05
	Port Nolloth	0.66	0.54
	Saldanha Bay	0.44	0.33
	Sea Point	0.69	-0.01
MUR	Lamberts Bay	0.60	0.29
	Port Nolloth	0.74	0.58
	Saldanha Bay	0.52	0.23
	Sea Point	0.63	0.42
G1SST	Lamberts Bay	0.73	0.32
	Port Nolloth	0.66	0.65
	Saldanha Bay	0.28	0.33
	Sea Point	0.57	0.30

The individual data products displayed different numbers of upwelling signals at distances of 0 km, 25 km, and 50 km from the coastline (**Figure 2.11**). There was no significant difference between the number of upwelling signals collected at the different sites (one-way ANOVA: $F = 2.27$, $d.f = 3$, SS = 2664, $p > 0.05$). However, there was a significant difference in the number of signals detected between products ($F = 53.53$, $d.f = 3$, SS = 13740, $p < 0.001$) and at different distances from the coastline ($F = 0.75$, $d.f = 2$, SS = 129, $p < 0.05$).

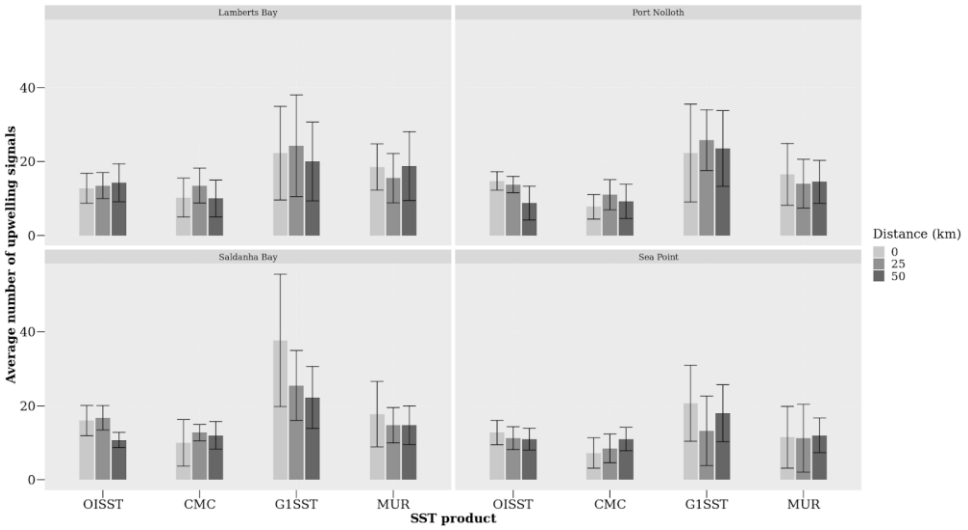

Figure 2.11: The average number of the signals detected at each site for the various satellite products.

2.4. Discussion

2.4.1 Data products

It was reported here that the highest resolution data, MUR and G1SST, which are available on a 0.01° grid, yielded the longest duration and cumulative intensity of upwelling signals compared to the coarser resolution data products. The MUR product, in particular, consistently yielded upwelling signals of the greatest intensity. Upwelling signals were most intense at the shore in all of the SST products. Analyses of the CMC, OISST and SACTN datasets revealed that recorded signals did not often exceed a duration of 10 days, whereas in MUR and G1SST the signals were detected for up to 14 days and even longer in some rare cases. Moreover, most of the signals detected in CMC, OISST and SACTN products only lasted for three days. This was similar for the higher resolution data products (G1SST and MUR) which also showed a high prevalence of signals lasting for just four days. In most cases, the number of signals detected at 0 km was higher than the number of signals detected at 50 km for the data products with the highest resolution. There was also a difference in mean intensity between products and distances from the site. The highest number of signals detected was recorded in the MUR and G1SST products.

Gridded datasets obtained from satellite imagery have provided an important understanding of offshore oceanographic processes and are reliable as they are usually spatially complete. However, coastal features such as upwelling cells are often smaller than the highest resolution of most SST products. In this study, estimates of upwelling duration, mean intensity and cumulative intensity (**Table 2.1)** may have been overestimated from data collected by the MUR and G1SST data products. These products are more likely to be susceptible to errors relating to limitations and data collection biases associated with satellite-derived sampling (Ricciardulli and Wentz, 2004; Liu et al, 2016), such as cases where there are large gaps within datasets that may have been caused by cloud cover or precipitation. These gaps are typically inferred from algorithms using past and forecasted data entries as well as data from nearby pixels which do not always reflect on real world patterns. For example, if upwelling signals were detected in an area that experienced extensive cloud cover over several weeks, the algorithm may suggest that upwelling continued throughout that period which may not have been the case. However, datasets constructed from multiple data sources, particularly from ships and buoys, are inherently more reliable in terms of reducing the frequency of falsely detecting signals as *in situ* help to prevent the SST algorithm from making interpolations away from reality (Smith and Reynolds, 2005; Kennedy et al., 2011). The overestimated data may be due to errors from different sources which are produced at each of the successive data processing level (Liu et al, 2016). For example, the Level 0 products (digitised detector output) to Level 4 products (bias corrected, geo-located, gridded, and gap-free SSTs). The SST accuracy refers to the retrieval error produced at Level 2 (derived SSTs at pixel bases), but Level 3 (binned, gridded and averaged Level 2 values) and Level 4 fields are extensively used in climate and modeling studies, mainly because of the desirable features of being “gridded and gap-free” (Liu et al, 2016). Another reason for this could be as a result of sampling error caused by incomplete coverage of satellite measurements. Cloudy pixels incomplete coverage may be due to the presence of clouds causing gaps in the sampling of SST. Cloudy pixels rejected by SST cloud masks constitute up to 90% of the total sampled pixels (Liu et al, 2016) and because of gaps between successive swaths of some sensors which may cause sampling errors.

It is important to note that the data sources are intrinsically different in the ways in which they were obtained or recorded. Consequently, discrepancies between datasets are to be expected. For example, the SACTN *in situ* collected SST product will reflect the actual temperature of the water being measured but instrumental differences when using a thermometer or an electronic sensor will result in inconsistencies. This is particularly prevalent because satellite temperatures are collected remotely and sensors do not make contact with the water. Here, properties of infrared (IR) and microwave (MW) are related through complex algorithms to temperature (Minnett et al., 2002). Smit et al. (2013) showed that warm and cold biases exist along the southern and western coastal region of South Africa, and the juncture between upwelling and non-upwelling regions have a tendency to influence the variability and magnitude of the SST bias. When comparing SST products, a small bias is always likely to be present because of cloud cover and wind strength (Dufois et al., 2012). Overall, the different data products compared within this study yielded different results. While flagging techniques are supposed to occasionally flag good values (Kilpatrick et al., 2001), it was found that flagging may occasionally be too vigorous for EBUS (Dufois et al., 2012). For example, the flagging method used on an OISST reference test induces warm coastal bias in data from both the MUR and G1SST data during summer. It should be noted that this phenomenon can be explained by strong coastal SST gradients in these upwelling regions. Differences in observations of upwelling events between data products at different sites, and at various distances from the coastlines can be attributed to several facets relating to the measurement protocols of each product. For example, differences in algorithms (Reynolds et al., 2002), components, and resolutions are contributed to the variable observation. Pixel-based atmospheric corrections developed for oceanic applications often fail or are inappropriate at the coast, and flagging techniques used to de-cloud data are also know to reduce strong biases at a monthly scale with strong horizontal SST gradients especially in upwelling systems. Missing pixels at the land/sea edge or 'land bleed'—i.e. pixels not flagged as missing but which are influenced by land temperatures 'mixing' with the actual sea temperatures may also influence temperature data obtained. Contributing towards the magnitude of differences in upwelling signals detected between the different SST products are factors such as data resolution, proximity from the coastline, the presence or absence of upwelling cells or embayments.

2.4.2. Oceanography

Upwelling processes in the southern Benguela are highly influenced by bottom topography (Nelson and Hutchings, 1983). The continental shelf which forms the eastern boundary of the Cape Basin, defined roughly by the 200 m isobath, varies in width from the 10 km at prominent capes to 150 km near Port Nolloth. In the vicinity of the Cape Peninsula and Cape Columbine, the coastline is irregular and two canyons associated with these features cut into the shelf, in the direction parallel to the coast (Nelson and Hutchings, 1983). However, along the remaining portion of the west coast, canyons are rare. The Cape Basin is bounded in the north by the Walvis Ridge which runs from the coast at 18° S to the Atlantic Central Ridge in a south westerly direction (Nelson and Hutchings, 1983). In the south, it is bounded by the Agulhas Ridge, a less pronounced topographic feature running parallel to the Walvsis Ridge from the Agulhas Plateau (Nelson and Hutchings, 1983). The dynamic topography of the area is such that the Agulhas Current water is fed into the Benguela systems from south of the Agulhas Bank.

Upwellling in the BUS occurs in a number of distinct upwelling cells, which form at location of maximum wind stress curl, and where there is a change in the orientation of the coastline. Lutjeharms and Meeuwis (1987) distinguished eight different cells (Cunene, Namibia, Walvis Bay, Lüderitz, Namaqua, Columbine, Cape Peninsula and the Agulhas cell), Shannon and Nelson (1996) further included three more upwelling cells along the south coast. The Lüderitz cell was identified as the most intense cell. Given that this research study is restricted to the southern Benguela, discrete upwelling cells at Cape Columbine and the Cape Peninsula will be discussed (Nelson and Hutchings, 1983). The Cape Columbine and Cape Peninsula upwelling cells are identified as two distinct bands of cold water on the inner and mid-continental shelves at a depth of 0-100 m, where upwelling is generally more intense during summer (Nelson and Hutching, 1983). This cold water is apparent along the length of the on the inner (0-100 m) and mid-continental shelves (100-200 m) (Weeks et al., 2006). A change in SST is present at Port Nolloth notable owing to the combined effects of being at the point of the southern limit of the Cape Peninsula upwelling cell and the sudden broadening of the inner shelf immediately to the south of the Peninsula. At the Cape Peninsula latitude, cooler upwelled water (<14°C) is confined primarily to the narrow inner shelf and this is evident in our data as we observe the most intense upwelling signals closer to the shore. It is also evident that the high resolution G1SST and MUR data sampled in Lamberts Bay, Saldanha Bay and Sea Point show the highest number of upwelling signals detected at the narrow inner shelf with fewer signals collected at the mid latitude shelf. The findings made here further show that the coarser resolution (OISST) product fails to pick up signals further offshore, as seen in Sea Point. Currie (1953) and Hart and Currie (1960) further explain that the BUS consists of a series of anticyclonic eddies of interlocking cool and warm water, which is in constant state of change. As a result, upwelling is not uniform along the coast and it is found upwelling water to originate between 200 and 300 m deep. By understanding the topography, it is evident that, although upwelling is not visible at the surface, subsurface upwelling is possible (Nelson and Hutching, 1983). This further suggests that in cases when the same signal was detected at the shoreline and 25 km from the coast, a corresponding signal would not be identified at a distance of 50 km and this may be explained by sub-surface upwelling.

While the SST data may be satisfactory for interpretation of regional phenomena; SST suffers from several drawbacks when applied within the coastal region. Here the interaction of hydrodynamic and atmospheric forces creates a complex system which is influenced by larger variability at smaller spatial scales than further offshore (Dufois et al., 2012). Hydrodynamic regimes such as stratified water columns may break down at the coast in very shallow waters, and seawater temperatures measured there may not directly relate to SSTs measured further from the coast at the ocean's surface (Broitman et al., 2008). These inshore hydrodynamics may be described by a) the injection of turbulence through breaking waves, thus increasing the breakdown of the mixed layer; b) convective mixing due to the cooling through the process of evaporation, which occurs during winter months under cool dry air; c) tidal mixing which minimises the vertical thermal gradient; and d) mixing through velocity often caused by wind driven currents. Together, these processes homogenise the first few meters of the water column and therefore minimise the difference between the surface temperature and deeper bulk temperature (Minnett et al., 2004). In hydrodynamically active zones, such as the BUS, the absence of shallow stratification would cause a portion of cooler water than the bulk surface waters of the ocean to which satellite SSTs have been referenced. Thermal heating of coastal waters may also be exaggerated due to the proximity to the coast (Dufois et al., 2012). This type of heating is commonly seen in embayments, which reduce water exchange and limit wave activity and ultimately affect the deepening of the thermocline. These processes are highly variable on a spatial and temporal scale depending on the coastal bathymetry and wind regime.

2.4.3 Conclusion

Despite the influence of many oceanographic factors affecting the detection of upwelling signals, SST generally shows a high degree of correspondence with measurements obtained by buoys and other sources of *in situ* seawater temperature measurements (Donlon et al., 2002; Smit et al., 2013). However, although SST products developed offshore and within the oceanic regions are being applied to the coastal regions, reports exist to inform users to exercise caution when using SST datasets in these coastal regions (Tittensor et al., 2010). It should also be noted that the patterns visible within this study region may result because of different scales in signals causing only higher resolutions to be able to detect them. Upwelling signals are small signals (cold pulses of water that may last for a few hours or days), which may have contributed to the higher resolution (MUR and G1SST) products detecting more signals lasting for a longer period when compared to the coarser resolution products (e.g. OISST). Finally, the MUR SST showed the most promise in terms of a reliable source for detecting and quantifying upwelling metrics as it was able to accurately detect the same signals visible at 0 km and 50 km from the coastline. However, in a case where long term (> 30 years) trends of upwelling signals are being studied, the OISST dataset would be more suitable as this time series extends for more than three decades.

Data products of the highest resolution yield upwelling signals more abundantly and intensely closer to the shore in the inner continental shelf region as expected given the topographical differences along the coastline. Hence, we conclude that the higher resolution data are more accurate at detecting these fine scale cold pulses. This research not only provides us with a better method of detecting upwelling signals, which is useful to observe trends in upwelling signals overtime, but also emphasizes the importance of selecting the correct data product in concert with knowledge about the nature of the physical phenomena being studied. Detecting and monitoring upwelling is a useful tool for ecosystem management and better characterisation of oceanographic processes. While this SST approach to upwelling shows promise, the limitations and biases within SST data collection methods as well as other factors of near shore versus offshore, oceanographic phenomena, and spatial resolution are all important considerations that must be taken into account.

CHAPTER 3

VARIATION IN UPWELLING SIGNALS DETECTED IN EBUS

Abstract

Global increases in temperature are altering land-sea temperature gradients. Bakun (1990) hypothesised that changes within these gradients will directly affect atmospheric pressure cells associated with the development of winds and will consequently impact upwelling patterns within ecologically important Eastern Boundary Upwelling Systems (EBUS). In this study we used daily timeseries of NOAA Optimally Interpolated sea surface temperature (SST) and ERA 5 reanalysis wind products to calculate a series novel of metrics related to upwelling dynamics. We then use these to objectively describe upwelling signals in terms of their frequency, intensity and duration throughout the four EBUS during summer months over the last 37 years (1982-2019). We found that a decrease (increase) in SST is associated with an increase (decrease) in the number of upwelling 'events,' a decrease (increase) in the intensity of upwelling, and an increase (decrease) in the cumulative intensity of upwelling, with differences between EBUS and regions within EBUS. The Humboldt Current is the only EBUS that shows a consistent response from north to south with a general intensification of upwelling. However, we could not provide clear evidence for associated changes in the wind dynamics hypothesized to drive the upwelling dynamics.

Keywords: Climate change, Upwelling, Seawater temperature, coastal regions, Code: R

3.1. Introduction

Coastal upwelling is a major oceanic process driven by prominent currents, of which those within Eastern Boundary Upwelling Systems (EBUS) are most important globally (Bakun and Nelson, 1991; Messié et al., 2009; Gruber et al., 2011; Pegliasco et al., 2015; Varela et al., 2015,2016,2018; Bonino et al., 2019; Brady et al., 2019). EBUS include the California (CCS), Humboldt (HCS), Canary (CnCS) and Benguela (BCS) current systems (**Figure 1**), with each of these significantly impacting their associated coastal ecosystems. These systems are present along the western shores of landmasses in the Pacific and Atlantic Oceans where they comprise vast regions of coastal ocean water (Bakun, 1990; Pauly and Christensen, 1995; Bakun et al., 2010; Santos et al., 2012a, 2012b; Bakun et al., 2015; Seabra et al., 2019). EBUS encompass a multitude of coastal regions stratified across several latitudes. Accordingly, these systems vary heterogeneously in terms of their environments and atmospheric conditions (Wang et al. 2015). As a result, variability within each EBUS naturally differs as the oceanic variables are driven by and respond to the combined effects of an assortment of differing oceanic and atmospheric processes and phenomena. For example, ocean temperatures within the CCS vary due to the combined effects of both El Niño-Southern Oscillation (ENSO) and Pacific Decadal Oscillation (PDO) (Jacox et al. 2015). Similarly, North Atlantic Oscillation (NAO), Benguela Niños, and Pacific ENSO are primarily responsible for driving variability in environmental conditions in the CnCs, BCS, and HCS respectively (Minobe et al., 1999; Chhak and Di Lorenzo, 2007; Di Lorenzo et al., 2008, García-Reyes et al., 2015; Gómez-Letona et al. 2017). One potential source of shared variability is suggested as stemming from anthropogenically-mediated climate change (Bakun, 1990), although the anticipated direction of the response remains uncertain (García-Reyes et al., 2015, Varela et al., 2018; Bonino et al., 2019), but no study, yet report shared variability and a consistent response across all EBUS (McGregor et al., 2007; Patti et al., 2010; Narayan et al.,2010, Pardo et al., 2011; Varela et al., 2015; 2018; Bonino et al., 2019). One potential source of shared variability is suggested as stemming from anthropogenically-mediated climate change (Bakun, 1990), although the anticipated direction of the response remains uncertain.

EBUS are a common focus of oceanographic and biological research because the complex interplay of biotic and abiotic processes within EBUS results in them being highly productive (Bakun, 1990; Pauly and Christensen, 1995; Tretkoff, 2011; Varela et al., 2015), diverse, and abundant in marine life. EBUS provide up to 20% of the world's fishery output despite only covering <1% of global ocean area (Bakun 2010; Bakun et al., 2015). Warm-season upwelling, driven by equatorial winds advected offshore by the Coriolis effect, is primarily responsible for the high levels of biological productivity present within EBUS (Huyer, 1983; Borges et al., 2003; Chavez and Messié, 2009; García-Reyes et al., 2010; Varela et al., 2018). These regions provide both lucrative economic (Costanza et al., 1997) as well as significant recreational services to people living along these coastlines, linking indirectly to the rest of the world. Recent studies have shown ecological changes in EBUS ecosystem structure (Fréon et al., 2009; Wang et al., 2015), hence monitoring these systems is becoming increasingly important. EBUS are formed in part by wind-driven ocean circulation, and their upwelling is dependent on wind direction and strength (Capet et al., 2004; Messié et al., 2015; Steinfeldt et al., 2015). Recognizing that alongshore winds that drive upwelling are initiated by changes in atmospheric pressure gradients at the cross-shore, Bakun (1990) hypothesized that long-term changes in climatic conditions would likely intensify continental oceanic pressure gradients (Bakun, 1990; Garcia-Reyes et al., 2015) and subsequently result in an increase in the frequencies and intensities of upwelling-favorable winds. Understanding, therefore, how these winds will change is of high importance for anticipating how upwelling might respond (Varela et al., 2015). For example, weaker upwelling may limit nutrient enrichment and potentially impact primary production (Figueiras et al., 2002; Chhak and Di Lorenzo, 2007; García-Reyes et al., 2015). In contrast, stronger upwelling may increase nutrient input and therefore offshore transport (Bakun et al., 2010, 2015). Increased wind intensity could also induce changes in water turbulence (Cury and Roy, 1989) which could affect chemical mechanisms and processes like ocean acidification and deoxygenation (Gruber, 2011) that may ultimately impact on productivity (García-Reyes et al., 2010). Elucidating on the drivers of upwelling and its relationship to nutrient enrichment and productivity could therefore inform conservation and facilitate management of fishers and other EBUS dependent resources. Such understanding is particularly important towards predicting the impacts of future climate change scenarios.

Recent reports from studies investigating patterns related to changes in upwelling winds have produced conflicting results, and a consensus on current trends has not been reached (Phillips, 2005; Bakun et al., 2010; Varela et al., 2015) This is largely due to contrasting findings regarding seasonal, interannual, and decadal fluctuations of unidirectional winds because of limited time series (Bonino et al., 2019; Seabra et al., 2019). Some researchers question whether the impacts of differential heating on the pressure gradient force drives intensification of coastal upwelling. Rather, a complementary hypothesis proposes that evidence of an intensifying pressure gradient force is limited to poleward migration of the Hadley Cell (Rykaczewski et al., 2015; Brady et al, 2017; Grise et al., 2019; Grise and Davis, 2020). Further complications preventing the agreement on findings in EBUS largely include a) researchers deriving conclusions from non-comparative datasets, b) data and analyses being treated in an inconsistent manner, c) variable quality between datasets, and d) inconsistencies in measurement techniques (Jacox et al., 2015; Bonino et al., 2019).

Upwelling has been investigated for several decades using a variety of statistical models and simulations (e.g. Bakun, 1990; Shannon et al., 1992; Bakun, 2010, Wang et al., 2015; Varela et al., 2015; Bonino et al., 2019). However, a

common theme among these attempts has been the broad temporal scale at which estimates were made. Most of studies on upwelling trends have used wind and temperature variables captured and averaged at monthly intervals. Here, we aimed to test the efficacy of a novel method for detecting upwelling signals and characterizing them in terms of intensity, frequency, and duration of upwelling 'events' in a manner that more reliably reflects real-world upwelling events. This is accomplished by using data at a fine temporal scale of daily intervals. In this context, the atmospheric and oceanic mechanics responsible for coastal upwelling are interdependent, and changes in one variable, such as wind speed, should directly affect variables such as upwelling intensity (Varela et al., 2015; 2016; Bonino et al., 2019). The objective of this study was to quantify the variation and changes in upwelling signals over time. The phenology of many marine ecosystem processes is highly affected and dependent on upwelling events such as its duration, frequency, and intensity (Barth et al., 2007). For example, intertidal communities require intermediate disturbance on rocky shores to maintain diversity (McGregor et al., 2007; Landry et al., 2009). Upwelling events may cause substantial or minimal disturbance depending on the frequency, duration, and intensity of the events (Benoit-Bird et al., 2019). However, upwelling also affects other marine communities and changes in upwelling patterns are likely to dramatically impact them (Wang et al. 2015). We therefore set out to detect if changes occur in the a) SST patterns, b) intensity, duration, and frequency of upwelling-favorable wind, and c) the frequency, mean, and cumulative intensity of upwelling signals during summer months over a period of 37 years. Understanding changes within these systems could allow for predictive management and conservation of fisheries and marine resources.

3.2. Methods

3.2.1. Data

To evaluate if there are changes in upwelling dynamics, this study used the gridded data of the global 0.25° National Oceanic and Atmospheric Administration (NOAA) daily Optimally-Interpolated Sea Surface Temperature (dOISST, v.2.1) (Reynolds et al., 2007; Banzon et al., 2016). This remotely-sensed satellite product has any gaps in spatial coverage filled through the interpolation of data collected from ships, and buoys (Reynolds et al., 2007; Banzon et al., 2016). The OISST data product has been collected for nearly four decades, hence providing us with a long (> 30 years) time series from which upwelling trends and their rate of change can be calculated. High resolution SST data sets are useful but often have limited time series. Most high-resolution data products (i.e. those with a resolution of ~0.01°) do not exceed 30 years in duration; for example, MUR (2002-2020) and G1SST (2010-2019). To detect variations in upwelling signals among the four EBUS (**Figure 1**) (Bakun, 1990; Bakun et al., 2015; García-Reyes et al., 2015; Varela et al., 2015; Varela et al., 2016, Sousa et al., 2017b), wind speed and direction were also necessary (see below). Wind speed and direction variables were downloaded from the ERA5 climate reanalysis produced by ECMWF, providing daily data on regular latitude-longitude grid at 0.25° × 0.25° resolution (C3S, 2017). Upwelling zones representative of each EBUS were selected according to previous studies (Sydeman et al., 2014; Varela et al., 2015, 2018; Seabra et al., 2019; Varela et al., 2020). Two upwelling systems were analyzed along the Eastern Atlantic Ocean, these are the Benguela Current (BCS: South 30.13–23.26°S, North 20.76–16.39°S) and Canary Current (CnCS: 18.89–32.63°N), and another two in the Eastern Pacific Ocean, including the Humboldt Current (HCS: Chile 37.62–28.88 °S, Peru 16.39–10.15 °S and California Current (CCS: South 33.88–36.06 °N, North 37.94–42.31 °N).

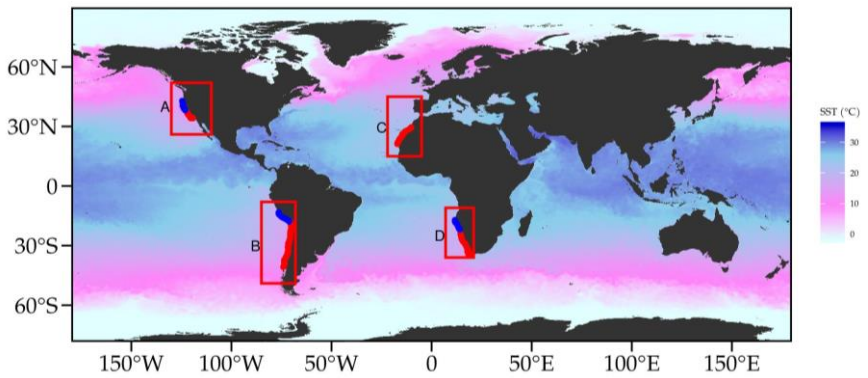

Figure 3.1: OISST throughout the global ocean. The red coloured rectangles delimit EBUS: A) California (CCS), B:) Humboldt (HCS), C) Canary (CnCS) and D) Benguela (BCS) current systems. Two upwelling systems were analyzed along the Eastern Atlantic Ocean, these are the A) Benguela (South 30.13–23.26°S; North 20.76–16.39°S) and Canary (18.89–32.63°N). Two upwelling systems were assessed in the Eastern Pacific Ocean, including the Humboldt Current (HCS: Chile 37.62–28.88°S, Peru 16.39–10.15°S) and California Current (CCS: South 33.88–36.06°N, North 37.94–42.31°N).

3.2.2. Upwelling identification

To identify whether changes exist in the frequency and intensity of upwelling signals across EBUS it must first be determined when upwelling occurs. To do this, a set of upwelling threshold values was needed to be established. Given that upwelling is primarily caused by alongshore, equatorward winds, both SST and wind data were used. Wind data were used to calculate the upwelling index using the formula presented in Fielding and Davis (1989):

$$upwelling\ index = \mu(\cos\theta - \tau).$$

Where μ represents the wind speed ($m.s^{-1}$), θ represents the wind direction in degrees, and τ is the orientation of the coastline (Jury 1980). This index relies on wind speed and direction to identify upwelling-favorable conditions. When the upwelling index is > 0, SST usually drop, as expected, suggesting that upwelling is occurring. Although previous authors did not demonstrate this lowering of SST. Here we established that the drop in SST that coincided with a positive upwelling index was close to the seasonally varying 25^{th} percentile threshold for SST. This threshold temperature was subsequently used in combination with the upwelling index to identify upwelling signals. With the upwelling index and SST threshold set, the detect_event() function from the **heatwaveR** package (Schlegel and Smit, 2018) was used to calculate metrics for the upwelling signals. By using this method of detecting signals, we were able to obtain upwelling metrics (**Table 3.1**) such as the frequency of occurrence, mean intensity, and cumulative intensity. Here, we defined the mean intensity (°C) as the mean temperature exceedance (i.e., duration below the 25^{th} percentile) during the upwelling signal. Cumulative intensity (°C.days) is defined as the sum of daily intensity exceedances across the duration of an event. Because upwelling signals were calculated relative to seasonal climatologies of percentile exceedances, rather than an absolute definition such as temperatures below a fixed temperature threshold, these signals could occur any time of the year; however, upwelling was proven to be more dominant during summer months, as expected. To quantify metrics of upwelling-favorable winds (i.e., southeasterly (SE) winds in the Southern Hemisphere and northeasterly (NE) winds in the Northern Hemisphere), we again made use of the detect_event() function. For these analyses, by setting the seasonality and threshold to a value of 0 allowed the statistical functions of the package to compensate for using wind data rather than SST data. This allowed us to estimate wind metrics such as the duration, intensity, and count of upwelling-favorable wind events within each of the regions.

Table 3.1: Metrics of upwelling signals and their descriptions.

Name (unit)	Definition
Count (n)	Number of upwelling signals per year
Mean intensity (°C)	Mean temperature anomaly during the upwelling signal
Cumulative intensity (°C.days)	Sum of the daily intensity anomalies over the duration of the signal

With upwelling being influenced by wind patterns, Bakun (1990) predicted that changes in wind patterns would influence the intensity of upwelling signals. As a first step, we calculated trends in SST to understand how temperatures within these cold-water regions are changing over time. We selected all coastal SST pixels along the latitudinal bands shown for each EBUS (**Figure 3.1**), as the coastal region is the most utilized for human habitation, leisure, recreational activities, or tourism. Given that the OISST time series length is greater than 30 years, it should be possible to discern long-term trends within the data from interannual noise (Hobday et al., 2016). Using linear regression analyses, we observed if there were changes in the number of times wind blew in an upwelling favorable direction, the duration of those winds, and their intensity, with an emphasis on austral (DJF) and boreal (JJA) summer months. The month variable was selected to observe which month expressed the most intense signal. To establish whether differences existed between currents and upwelling metrics over time, we assessed the upwelling metrics as a function *year* or *month*. Thereafter, using regression analysis, we compared the mean numbers of upwelling signals detected in each of the currents.

3.3. Results

Our investigations of trends in upwelling metrics across individual time series for each of the EBUS currents revealed the presence of noticeable shifts in SST patterns at each EBUS over the past 37 years (**Figure 3.2, A, B**). We found that SST dramatically differed across each EBUS (two-way ANOVA: $F = 1878.76$, $SS = 6966$, $p < 0.05$). This was in part driven by variable increases in SST in the BCS North (**Table 3.2**). Conversely, the BCS South and HCS showed a significant decrease in SST (**Table 3.2**). We further found a significant negative trend in monthly SST within the HCS, specifically during the months of January near Chile ($R^2 = 0.01$, slope = -0.2 °C.dec^{-1}, $p < 0.05$) and during December near Peru ($R^2 = 0.03$, slope = -0.4 °C.dec^{-1}, $p < 0.05$).

Table 3.2: Results from linear regressions in upwelling favorable winds and upwelling metrics over a period of 37 years. Positive trends are prefixed with a (+) shown with red text and negative with a (-) and appear in blue.

EBUS	Benguela Current South	Benguela Current North	Humboldt Current Chile	Humboldt Current Peru	California Current South	California Current North	Canary Current
SST ($°C.dec^{-1}$)	**(-) R^2 = 0.02, slope = -0.12, $p < 0.05$**	**(+) R^2 = 0.12 slope = 0.14 $p < 0.001$**	**(-) R^2 = 0.08 slope = -0.08 $p < 0.001$**	**(-) R^2 = 0.08 slope = -0.12 $p < 0.01$**	R^2 = 0.02 slope = 0.02 $p > 0.05$	R^2 = 0.01 slope = -0.02 $p > 0.05$	R^2 = 0.02 slope = 0.03 $p > 0.05$
No. of upwelling signals ($count.dec^{-1}$)	R^2 = 0.02 slope = 0.03 $p > 0.05$	**(-) R^2 = 0.15 slope = -0.10 $p < 0.05$**	**(+) R^2 = 0.10 slope = 0.10 $p < 0.05$**	**(+) R^2 = 0.05 slope = 0.10 $p < 0.005$**	R^2 = 0.001 slope = -0.02 $p > 0.05$	R^2 = 0.01 slope = -0.02 $p > 0.05$	**(-) R^2 = 0.06 slope = -0.05 $p < 0.005$**
Mean intensity ($°C.dec^{-1}$)	**(-) R^2 = 0.02 slope = -0.05 $p < 0.05$**	**(+) R^2 = 0.02 slope = 0.04 $p < 0.01$)**	**(-) R^2 = 0.006 slope = -0.03 $p < 0.001$**	**(-) R^2 = 0.01 slope = -0.05 $p < 0.05$**	(0) R^2 = 0.03 slope = 0.001 $p > 0.05$	**(-) R^2 = 0.001 slope = -0.01 $p < 0.001$**	**(+) R^2 = 0.03 slope = 0.01 $p < 0.05$**
Cumulative intensity ($°C.days.dec^{-1}$)	**(-) R^2 = 0.001 slope = -0.40 $p < 0.001$**	**(+) R^2 = 0.02 slope = 0.70 $p < 0.001$)**	**(-) R^2 = 0.001 slope = -0.003 $p < 0.05$)**	**(-) R^2 = 0.001 slope = -0.08 $p < 0.05$)**	(0)R^2 = 0.000, slope = -0.06 $p > 0.05$	**(-) R^2 = 0.01 slope = -0.20 $p < 0.05$**	(0) R^2 = 0.003 slope = -0.05 $p > 0.05$
No. of upwelling-favorable wind ($count.dec^{-1}$)	R^2 = 0.002 slope = -0.01 $p > 0.05$	R^2 = 0.003 slope = 0.02 $p > 0.05$	R^2 = 0.009 slope = 0.005 $p > 0.05$	R^2 = 0.004 slope = -0.011 $p > 0.05$	R^2 = 0.03 slope = 0.02 $p > 0.05$	**(-) R^2 = 0.04 slope = -0.008 $p < 0.05$**	R^2 = 0.000 slope = 0.003 $p > 0.05$
Wind duration ($days.dec^{-1}$)	R^2 = 0.001 slope = 0.01 $p > 0.05$	R^2 = 0.01 slope = -0.08 $p > 0.05$	R^2 = 0.003 slope = 0.02 $p > 0.05$	R^2 = 0.0002 slope = 0.03 $p > 0.05$	R^2 = 0.01 slope = 0.01 $p > 0.05$)	R^2 = 0.004 slope = -0.009 $p > 0.05$	R^2 = 0.002 slope = -0.08 $p > 0.05$
Wind intensity ($m.s^{-1}.dec^{-1}$)	R^2 = 0.02 slope = 0.01 $p > 0.05$	R^2 = 0.03 slope = 0.02 $p > 0.05$	R^2 = 0.006 slope = -0.01 $p > 0.05$	R^2 = 0.01 slope = 0.01 $p > 0.05$	R^2 = 0.02 slope = 0.08 $p > 0.05$	R^2 = 0.001 slope = 0.02 $p > 0.05$	R^2 = 0.03 slope = 0.03 $p > 0.05$

The numbers of upwelling signals decreased over time in the BCS North and CnCS, but slightly increased in HCS (**Figure 3.2, B**). Increases in detections were particularly prominent when SST decreased (**Figure 3.2, A**). A regression analysis showed a significant negative trend in the number of upwelling signals detected in the BCS North and CnCS (**Figure 3.2, C**). However, a positive trend is present in HCS Chile, HCS Peru. Conversely, a significant positive trend was detected in the mean intensity of upwelling in the BCS North and CnCS (**Table 3.2**). Results of a linear regression showed significant negative trends in the mean intensity of upwelling signals in the BCS South, HCS Chile and Peru and CCS North. We also found that the cumulative intensity of upwelling signals significantly differed between the EBUS (ANOVA: $F = 371.15$, $SS = 178853$, $p < 0.05$) and between month (ANOVA: $F = 139.78$, $SS = 123484$, $p < 0.05$; **Figure 3.2, D**). Results of a linear regression showed significant negative trends in cumulative intensity within the BCS South, HCS Chile and Peru and CCS North.

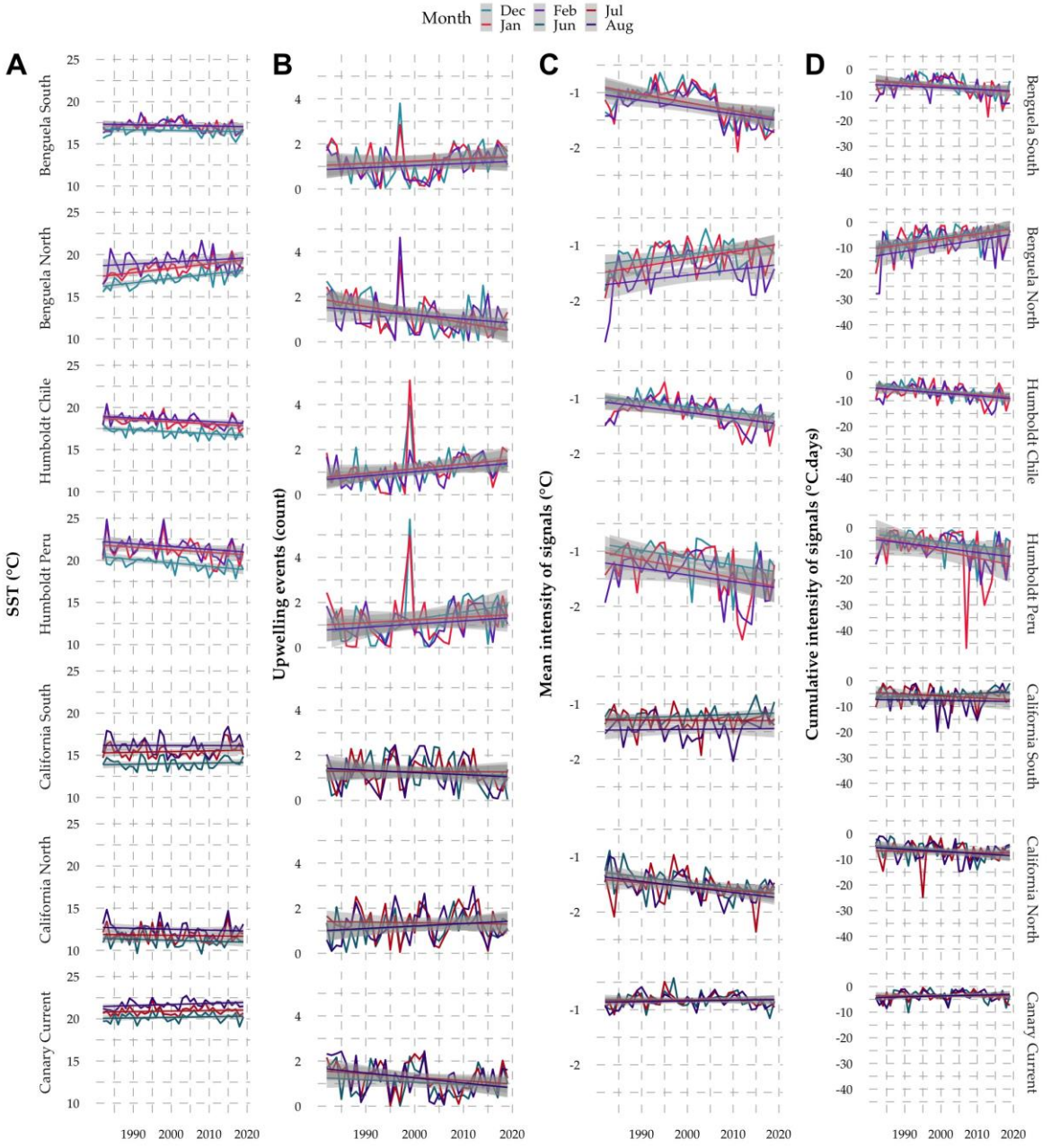

Figure 3.2: SST trends and count, mean, and cumulative intensity of upwelling signals during austral (DJF) and boreal (JJA) summer months over a period of 37 years. Where a more negative intensity represent a more intense signal.

Counts of discrete upwelling-favorable wind events were not uniform among the four EBUS (**Figure 3.3,A**). A two-way ANOVA analysis showed a significant difference in upwelling-favorable wind events between currents ($F = 1878.76$, $SS = 6966$, $p < 0.05$). However, a regression analysis showed no significant changes in wind events detected over the past 37 years; the CCS North was the only exception showing a significant negative trend in upwelling-favorable winds (**Table 3.2**). A significant positive trend was detected in the number of monthly upwelling-favorable winds during July in the CCS South ($R^2 = 0.25$, slope = 0.05 count.dec^{-1}, $p < 0.05$) and during February in the HCS Chile ($R^2 = 0.14$, slope

= -1.1 count.dec^{-1}, $p < 0.05$) within the HCS. A significant negative trend was present during December within the HCS ($R^2 = 0.10$, slope = -1.1 count.dec^{-1}, $p < 0.05$).

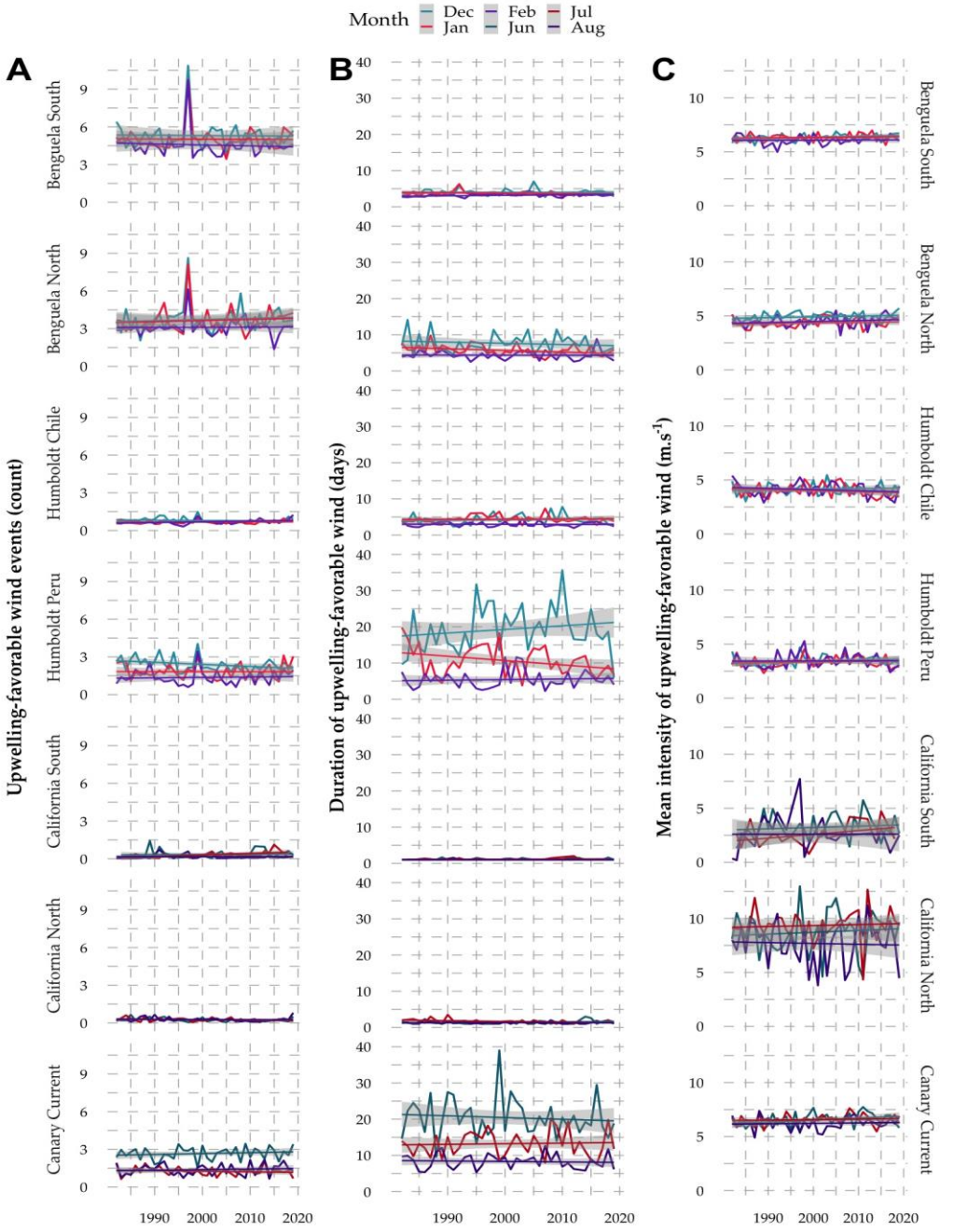

Figure 3.3: Duration, count, and mean intensity of upwelling-favorable winds during austral (DJF) and boreal (JJA) summer months over a period of 37 years.

The typical duration of south-easterly winds in the BCS and HCS Chile ranged between 3 – 6 days with the the HCS Peru being the only exception with a duration >10 days (**Figure 3.3, B**). Upwelling-favorable winds in the CCS often did not exceed two days, except for the CnCS with an average duration of 14 days (**Figure 3.3, C**). Results of an ANOVA analysis showed a significant difference in the duration of upwelling-favorable winds between the EBUS regions ($F = 431.29$, $SS = 16113$, $p < 0.005$) (**Table 2**). A significantly negative monthly trends in wind duration during July months in the CCS North ($R^2 = 0.004$, slope = -0.2 days.dec^{-1}, $p < 0.05$) and during January in the HCS Peru ($R^2 = 0.008$, slope = -1.1 days.dec^{-1}, $p < 0.05$) was detected. Upwelling-favorable winds appeared to be most intense in the CCS North, often exceeding 7 m.s^{-1} (**Figure 3.3, D**). Winds were least intense in the CCS South with a speed of approximately 4 m.s^{-1} being commonplace (**Figure 3.3, C**). There were no significant changes in the overall wind intensity over time within the EBUS regions (**Table 2**). A regression analysis comparing wind intensity per month, however, showed a significant change during July in the CnCS ($R^2 = 0.01$, slope = 0.10 m.s^{-1}.dec^{-1}, $p < 0.05$). We also found no significant change in the wind intensity of EBUS over time **(Table 2)**.

3.3. Discussion

Bakun (1990) hypothesized that an increase in greenhouse gases will result in considerable changes in land-sea pressure gradients that will affect global wind patterns and ultimately result in an increase in the intensity of upwelling across the world's oceans. We tested this hypothesis by analyzing upwelling trends at four prominent coastal upwelling regions, with an emphasis on austral (DJF) and boreal (JJA) summer months as this is when upwelling is most prevalent. By combining wind and SST data we were able to observe trends in upwelling responses. Specifically, change in upwelling metrics—as established by our novel methodology—was ubiquitous across all four EBUS. Trends in the metrics are coupled such that we see a decrease (increase) in SST coupled with a concurrent increase (decrease) in the number of upwelling 'events' and an increase (decrease) in the mean and cumulative intensity of upwelling. However, the change was inconsistent across the upwelling regions. In terms of the SST response, the Humboldt Current off Peru and Chile and the southern Benguela Current displayed decreases of ~0.37°C and 0.44°C during past 37 years, while in the northern Benguela Current region it increased by ~0.52°C during this time. No significant changes were observed for the Canary California Currents in the northern hemisphere. Surprisingly, it was interesting that anticipated changes in the decadal trend in mean intensity, duration, and count of upwelling-favorable winds were generally not detected. The significant cooling trend of the southern region of the Benguela Current is in agreement with previous research (Lima and Wethey, 2012; Santos et al., 2012a) that suggested that these decreases were related to increased upwelling. Further, at the southern end of the Benguela Current the highest upwelling intensities were observed during summer seasons (Narayan et al., 2010; Patti et al., 2010). Other studies (for example Cropper et al., 2014; Varela et al., 2015; Benazzouz et al., 2015; Santos et al., 2016; Varela et al., 2020) demonstrated that a cooler SST associated with an increase in upwelling in coastal areas, as was also observed in Chile and Peru in this study. Previous studies demonstrated that trends in upwelling along the Peru coastline were variable. Here we report no significant change in upwelling-favorable winds along the Peru coastline, which contrasts with the studies reported by Gutierrez et al. (2011) and Varela et al. (2015). The California Current displayed a positive trend in the mean intensity of upwelling signals over time, which is in disagreement to the study conducted by Varela et al. (2015). Here we also report no significant trend in wind speed, which contrasts with the studies reported by Mendelssohn and Schwing (2002), Narayan (2010) and Garcia-Reyes and Largier (2014). The Canary Current displayed increases over time in metrics indicative of upwelling-favorable wind (Narayan et al., 2010; Patti et al., 2010), but apparently without an associated change in upwelling. Our findings here, and the findings of the aforementioned studies, suggest that warming rates are generally depressed along the coast within upwelling regions (Santos et al., 2012a; 2012b), but we show that this seems to be the case for the southern hemisphere upwelling systems only (excluding the northern Benguela Current where it is increasing).

Using our novel method of determining upwelling signals, our results do not support the hypothesis that intensified upwelling will result from the increased land-sea temperature difference associated with climate change. However, it is possible that natural multi-decadal scale climate variability impacted the trends discussed. For example, the occurrence of ENSO at the end of the time series could also have initiated an anomalously warm SST in EBUS and potentially affected the trends observed. These results also lead to discussion about the potential connection between ENSO within EBUS and the Benguela Niño in the Benguela Current (Peterson and Schwing, 2003; Blamey et al., 2012; Sydeman et al., 2013). ENSO represents a weakening of the Walker cell circulation (Wang, 2004). During normal Walker cell conditions there is consistent upwelling, and this upwelling contributes to cool SST (Bakun, 2010). Since the Canary Current show an increase in SST, it may suggest that there has been a weakening or reversal of the trade winds as has been indicated by earlier studies (Vallis 1986; Saji et al., 1999). ENSO drives atmospheric and oceanic Rossby waves that can influence climate processes (Battisti, 1989; Holbrook et al., 2011). The ENSO's counterpart, La Niña, produces a teleconnection that alters the mean climatic states (Diaz et al., 2001; Fogt and Bromwich, 2006; Yeh et al., 2018). As a result, it can also be reasoned that the fewer upwelling signals are detected in Chile and Peru is potentially a consequence of the effects of La Niña. During La Niña, the Walker cell circulation is enhanced (Sohn et al., 2013), meaning that pre-existing trade winds and SST strengthen. The low SSTs created by the presence of La Niña are accompanied by anticyclones. The anticyclones rotate counterclockwise in the southern hemisphere, and therefore its winds travel equatorward where they move surface water away from the shore, resulting in a net Ekman veering that encourages coastal upwelling and lowers SST (Alford, 2001).Given these results, the need to consider changes in both thermal and in-shore hydrodynamic processes such as wind driven currents when interpreting the full dynamical response such as in conditions of changing wind magnitude and direction of the coupled atmospheric-ocean system to climate warming is important. In this regard, our conclusion differs in respect to recent studies (e.g. Wang et al., 2015) that have examined the relationship between increasing summertime land-sea temperature differences and intensified upwelling in response to climate change. Rykaczewski et al. (2015) recommended that expanded land-sea temperature contrasts are omnipresent in projections of future conditions, but that summertime upwelling is limited to the polar extremes of upwelling zones. If true, this would indicate that increased land-sea temperature differences do not have a dominant influence on upwelling intensity (Tim et al., 2015; Tim et al, 2016). Additionally, changes in upwelling-favorable winds are not always directly related to broad increases in land-sea temperature differences associated with climate change (Rykaczewski et al., 2015). Research suggests that changes in sea level pressure (SLP) fields are expected in response to increased greenhouse gas concentration (Gillett et al., 2013). These shifts will initiate changes

in the magnitude, location and timing of upwelling-favorable winds that are more consequential than increased land-sea temperature differences.

Simulations of ocean patterns in the Benguela Current using high resolution data over the past few decades have thus far failed to detect predicted intensification of upwelling. For instance, Tim et al. (2015) demonstrate that upwelling has not dramatically intensified over at least the past 50 years. Moreover, broader investigations of global climate changes have also failed to detect meaningful intensification patterns of upwelling and in addition have not forecasted that such intensification will occur in the future (Wang et al. 2015; Tim et al. 2016). One potential reason for our results contrasting with the predictions by Bakun (1990) could be that the differences in quality of wind data employed were too severe. Bakun (1990) used Wave and Anemometer-based Sea surface Wind (WASWind) data whereas we made use of ERA5 climate reanalysis. Both datasets are biased to some degree. WASWind data are based on ship-based measurements and were fund to produce an artificial upwards trend in in sea surface wind speeds due to variable increases in the heights of anemometers (Tokinaga and Xie, 2011). These data have since been corrected, and the trends expressed by Bakun (1990) are no longer applicable with the corrected wind data, at least in some regions such as Peru (Belmadani et al., 2014). ERA5 climate reanalysis data are also susceptible to several biases (see Astudillo et al., 2017; Taboada et al., 2019) but are considerably more accurate and reliable given the spatial and temporal resolution at which winds are measured (Graham et al., 2019; Mayer et al., 2019; Tetzner et al., 2019). For comparison, ERA5 products are provided daily at a 0.25° × 0.25° latitude-longitude and are available from 1979 to present, whereas WASWind data are available at monthly intervals at 4° × 4° latitude-longitude resolution and cover the years from 1950 – 2008. One potential caveat of our analysis and the interpretations thereof lays in the limited nature of the time series we assessed. Because we sought to detect and quantify patterns of upwelling at a fine spatio-temporal scale, our choice in datasets was limited to high-resolution data that only cover the past 37 years. In the context of broader climate change, 37 years is likely too short a duration of time from which to inform long-term shifts in patterns of global phenomena like upwelling and so our findings here should be regarded with some caution. While we cannot provide evidence in support of Bakun's hypothesis regarding intensification of upwelling (Bakun 1990), we cannot rule out the possibility that an analysis with longer time series could produce a different outcome. Unfortunately, high-resolution SST datasets that cover longer time periods do not exist. Some longer reanalysis products like ERA20C or 20CR provide data over a time series of more than 100 years but these data products are only available at a considerably coarser resolution and may not be suitably sufficient to reliably estimate upwelling.

There is not yet an adequate amount of data to effectively investigate the effects of changes in climatic conditions on coastal SSTs and biogeochemistry in the EBUS (García-Reyes et al., 2015). Despite this, consideration is now given to changes in terms of the location and intensity of upwelling due to its necessity for the identification of high-risk regions of the coast that are prone to processes such as ocean acidification, increased hypoxia, and eutrophication which have been projected in accordance with future warming (Rykaczewski et al., 2015). These patterns are affected by both complex global and local processes; however, the availability of the data and their corresponding resolution in conjunction with a wide range of decadal temperature variability and biogeochemical properties also play a significant role. Most of the remotely sensed SST and wind products do not have sufficient resolution to accurately detect nuances within the upwelling process. Despite this, data providers have been yielding promising advancements in higher resolution products by using land and air-sea interactions, cloud formation, and oceanic mesoscale processes to correct the biases presented in older sources. It has since become necessary to take into consideration changes in local, alongshore winds when investigating the relationship between sensitivity of upwelling and climate change (Bakun et al., 2015). Environmental variables that drive upwelling like temperature and wind measures are highly variable in EBUS regions, both spatially and temporally. Changes in these variables are shown here to directly affect upwelling patterns. As a result, major shifts in these drivers can greatly influence the frequencies, intensities, and the durations of upwelling events. Increases and decreases in SST are negatively associated with corresponding shifts in detected upwelling. Similarly, heterogeneous winds can dramatically influence upwelling responses. Accordingly, it is vital to take into consideration both the geostrophic and ageostrophic processes that affect the boundary layer of the coastal ocean when investigating upwelling. By analyzing these coupled processes, researchers can further elucidate upon the drivers that regulate changes in the characteristics of upwelling events. This is especially true since changes in water-column stratification can distort upwelling signals (Roemmich and McGowan, 1995; Chhak and Di Lorenzo, 2007) and so external processes like wind direction are important to consider. However, we found that the dynamics of upwelling-favorable winds have not changed significantly over the past 37 years. Further analyses may be required to fully interrogate the effects of shifts in climate on upwelling dynamics in EBUS.

In this study we produce metrics that track the duration and intensity of upwelling signals over the past 37 years. These metrics are based in part on those used to quantify marine heatwaves (Hobday et al., 2016; Schlegel and Smit, 2018) and they offer a valuable new approach that can be used to determine the changing dynamics of upwelling consistently and objectively in daily timeseries of SST and winds. While all four EBUS experienced some change in upwelling metrics, only those in the southern hemisphere generally responded with a decrease in SST (the northern Benguela Current region trended upwards). Although decreases in SST were associated with corresponding changes in upwelling intensity, a trend in wind dynamics apparently did not explain the upwelling dynamical response. We thus follow in the long tradition of not being able to conclusively support Bakun's (1990) hypothesis. Continuing shifts in climate may

indeed facilitate increased upwelling in certain coastal areas and thus buffer ecosystems from climate change (Bakun, 1990; 2010; García-Reyes et al., 2015), but it seems that this might not be seen consistently across all EBUS. The degree to which all EBUS can be characterized as resilient and robust to natural climate variability remains uncertain, as is the universal benefit of upwelling intensification to maintaining an abundance of species of high commercial and conservation value (Bell et al., 2015; Wilson and Forsyth, 2018). However, given the coarse resolution of current climate models for ocean variables, it is difficult to reproduce the relatively fine-scale upwelling features necessary for such research at present (García-Reyes et al., 2015). Continuing development of geophysical time series in the future will likely yield data series that are better able to yield trends indicative of climatic change. The knowledge of future changes in upwelling systems is a key factor for estimating changes in economic and biological trends. The metrics of intensity and duration of upwelling (and of frequency of upwelling 'events' that can be also established using our approach) will more than likely also relate to a diversity of measures of ecological functioning and well-being and provide researchers with another tool to track environmental drivers and responses.

CHAPTER 4

SYNTHESIS AND CONCLUSION

In the first study of this thesis, I used SACTN *in situ* collected data and satellite SST products to identify and compare upwelling signals at a variety of distances from the coastline. Here upwelling signals were used as a known signal in the data and allowed for a comparison between data products to quantify the efficacy of data products of differing resolutions. My findings here demonstrated the differences between SST products and their various resolutions. After demonstrating the capacity to identify upwelling signals using a novel method in the first study, the second study focussed on quantifying trends relating to upwelling signals within ecologically important EBUS currents over the past 37 years. Bakun (1990) proposed that climate change resulting from increased quantities of greenhouse gasses may fundamentally alter pressure gradients that will affect wind patterns and ultimately increase upwelling over prolonged periods. My results obtained from this study could not support Bakun's hypothesis. Importantly, the method used here differs from previous methods of identifying upwelling and currently represents the most effective means for identifying metrics of upwelling.

4.1. Contributions

I have presented a new method of detecting upwelling using SST and wind variable data. Prior studies on the matter, such as seen in Fielding and Davis (1989), often only consider wind measures to determine an upwelling index. My proposed method expands upon this by also including measures of SST, allowing for upwelling events as being defined when there were simultaneous drops in SST and a positive upwelling index. By using the `detect_event()` function in the **heatwaveR** package ((Schlegel and Smit, 2018) I was able to obtain distinct upwelling metrics (such as, mean intensity, cumulative intensity and duration) for each signal. This technique is useful as these quantifiable parameters can be calculated in an objective and consistent manner irrespective of geographical location. With these metrics, I was able to compare patterns in upwelling signals over time. The cumulative intensity metrics is perhaps the most important ecologically. As a product of duration and intensity, cumulative intensity can be used as an index to measure the threat of reduced upwelling on coastal systems. In Chapter 2, I used this method of determining upwelling, i.e. to compare differences in the counts, intensity and duration of upwelling signals at various distances from the coastline, and identified where upwelling was more dominant and intense. Using this method in Chapter 3, I identified signals which allowed me to observe patterns of upwelling within the world's four EBUS. Given the variable nature of my results, it became evident that further considerations on thermal and hydrodynamic processes relating to the upwelling process should be taken into account in future research that refines the process I developed above.

As seen in Chapter 2, the higher resolution data, the Group for High Resolution Sea Surface Temperature (G1SST) and Multi-scale Ultra-high Resolution (MUR) data products, detected signals lasting considerably longer and with higher cumulative intensity compared to the Optimally-Interpolated Sea Surface Temperature (OISST), Canadian Meteorological Center (CMC) and South African Coastal Temperature Network (SACTN) data products. The results also showed that upwelling varied at different distances from the coastline and that the higher resolution data would more likely detect upwelling further from the coastline compared to the lower resolution data. However, while higher resolution data produced overall superior detections, the limitations of the data products of broader resolutions did not severely alter the findings, although the effects due to data resolution were noticeable. The bathymetry within the Benguela Current region also plays an important role in affecting the detection of upwelling signals. Cooler upwelling waters are confined primarily to the narrow shelf allowing abundant and more intense upwelling to occur closer to the shore, and hence future research should primarily incorporate higher resolution datasets as these data are less likely to have incorrect readings and biases because they are obtained at a finer scale resulting in a more accurate product. Patterns obtained will then be more realistically reflected and minimise the likelihood of exaggerated detections.

By observing patterns of upwelling signals in EBUS for a period of 37 years, it is evident that the effects of anthropogenic changes towards altering upwelling intensity is more complex than proposed in the Bakun (1990) hypothesis. Here I show SST increased during summer months in all EBUS, except for the Humboldt current system (HCS). With this rise in SST, the number of upwelling signals appeared to have decreased over time, except for the HCS where an increase in the number of upwelling signals seemed apparent. The recorded increase in SST and decrease in upwelling signals is restricted to the surface as measured by the remotely sensed products *In situ* observations are required to test whether this results are evident throughout the water column. I also showed that the intensity of upwelling signals did not increase over time in three of the four EBUS, with the CnCS being the exception. More importantly, wind patterns within the EBUS did not intensity over time as speculated by Bakun (1990). The mean intensity of upwelling showed a negative trend in three of the EBUS, with the CnCS being the only exception with showcasing a slight positive trend. It is also highly likely that a natural climatic variable (not accounted for in this study) impacted the trends observed in this study. For example, ENSO could have initiated anomalously warm SST when observing these trends.

4.2. Further research

The past decade has experienced development of several remotely-sensed SST products and blends of *in situ* and satellite data from diverse sources into a gap-free products useful to the marine science community. These products are under continuous revision, and each analysis enhances the quality of the data as algorithms are refined and the biases within the data are understood in more detail. Given that many factors that can influence how well SST products reflect climatological reality, several data products were used in this study to compensate for limitations and biases. However, because the data are collected at different resolutions, it is unsurprising that there are large discrepancies between data products. Satellite-derived data are obtained using instruments that are never in contact with the water, and hence the biophysical properties are sometimes related through inadequate algorithms to temperature. Further studies should aim at improving the proximity at which reliable data can be collected to the shore, which would enhance the detection of localised upwelling cells closer to the shoreline.

To better test the hypotheses proposed by Bakun (1990), future research should also seek to incorporate sea level pressure data and its trends over time within EBUS. This should be done by observing summertime intensification between the temperature gradient and modifications to sea level pressure. As with many scientific fields, a greater knowledge of a subject often raises further questions which need answering. A range of further questions and data gaps were identified throughout my thesis. Understanding upwelling variability is important to assess marine ecosystem health, including that of factors such as ocean acidification and deoxygenation. Although the importance of upwelling is clear, reasons for the changes in upwelling metrics and the impact of anthropogenic climate change on these ecosystems are unclear. Changes in upwelling (count, metrics and duration) could affect marine ecosystems by influencing nutrient content into the euphotic zones if primary production is nutrient-limited. Changes in the phenology in upwelling winds may also affect trends within and across ecosystems as described here. Additionally, variation in the timing of upwelling strongly influences ecosystem productivity. Further research efforts should also focus on improvement of the methodology employed here to understand and include both atmospheric and oceanographic states during upwelling. The main goal of this thesis was not to predict events or signals but rather to use this novel method of determining upwelling signals and conduct an investigation into changes in trends in upwelling patterns over time. Ultimately the forecasting of upwelling signals should be used in conjunction with the adoption of subsequent future policies to better prepare for changes in these phenomena.

REFERENCES

Aguirre, C., Rojas, M., Garreaud, R.D., Rahn, D.A., 2019. Role of synoptic activity on projected changes in upwelling-favourable winds at the ocean's eastern boundaries. *npj Climate and Atmospheric Science*, *2*(1), pp.1-7.

Alves, J.M., Miranda, P.M., 2013. Variability of Iberian upwelling implied by ERA-40 and ERA-Interim reanalyses. *Tellus A: Dynamic Meteorology and Oceanography*, *65*(1), p.19245.

Arístegui, J., Álvarez-Salgado, X. A., Barton, E. D., Figueiras, F. G., Hernández León, S., Roy, C., & Santos, A. M. P. (2006). Oceanography and fisheries of the Canary Current Iberian region of the Eastern North Atlantic.

Arístegui, J., Barton, E.D., Álvarez-Salgado, X.A., Santos, A.M.P., Figueiras, F.G., Kifani, S., Hernández-León, S., Mason, E., Machú, E., Demarcq, H., 2009. Sub-regional ecosystem variability in the Canary Current upwelling. *Progress in Oceanography*, *83*(1-4), pp.33-48.

Arntz, W.E., Gallardo, V.A., Gutiérrez, D., Isla, E., Levin, L.A., Mendo, J., Neira, C., Rowe, G.T., Tarazona, J., Wolff, M., 2006. El Niño and similar perturbation effects on the benthos of the Humboldt, California, and Benguela Current upwelling ecosystems. *HAL archives-ouvertes.*

Auad, G., Miller, A. and Di Lorenzo, E., 2006. Long-term forecast of oceanic conditions off California and their biological implications. *Journal of Geophysical Research: Oceans*, *111*(C9).

Bakun, A., 1990. Global climate change and intensification of coastal ocean upwelling. *Science*, *247*(4939), pp.198-201.

Bakun, A., Nelson, C.S., 1991. The seasonal cycle of wind-stress curl in subtropical eastern boundary current regions. *Journal of Physical Oceanography*, *21*(12), pp.1815-1834.

Bakun, A., 1996. Patterns in the ocean: ocean processes and marine population dynamics, 323 pp. *University of California Sea Grant, San Diego & Centro de Investigaciones Biológicas del Noroeste, La Paz*.

Bakun, A., Weeks, S.J., 2004. Greenhouse gas buildup, sardines, submarine eruptions and the possibility of abrupt degradation of intense marine upwelling ecosystems. *Ecology Letters*, *7*(11), pp.1015-1023.

Bakun, A., Field, D.B., Redondo-Rodriguez, A.N.A., Weeks, S.J., 2010. Greenhouse gas, upwelling-favorable winds, and the future of coastal ocean upwelling ecosystems. *Global Change Biology*, *16*(4), pp.1213-1228.

Bakun, A., Black, B.A., Bograd, S.J., Garcia-Reyes, M., Miller, A.J., Rykaczewski, R.R. and Sydeman, W.J., 2015. Anticipated effects of climate change on coastal upwelling ecosystems. *Current Climate Change Reports*, *1*(2), pp.85-93.

Barange, M., Gibbons, M.J., Carola, M., 1991. Diet and feeding of Euphausia hanseni and Nematoscelis megalops (Euphausiacea) in the northern Benguela Current: ecological significance of vertical space partitioning. *Marine Ecology Progress Series*, pp.173-181.

Barth, J.A., Menge, B.A., Lubchenco, J., Chan, F., Bane, J.M., Kirincich, A.R., McManus, M.A., Nielsen, K.J., Pierce, S.D. and Washburn, L., 2007. Delayed upwelling alters nearshore coastal ocean ecosystems in the northern California current. *Proceedings of the National Academy of Sciences*, *104*(10), pp.3719-3724.

Barton, E.D., Field, D.B., Roy, C., 2013. Canary current upwelling: More or less?. *Progress in Oceanography*, *116*, pp.167-178.

Barton, C.A., McCormack, J.P., Eckermann, S.D., Hoppel, K.W., 2019. Optimization of Gravity Wave Source Parameters for Improved Seasonal Prediction of the Quasi-Biennial Oscillation. *Journal of the Atmospheric Sciences*, *76*(9), pp.2941-2962.

Battisti, D.S., 1989. On the role of off-equatorial oceanic Rossby waves during ENSO. *Journal of physical Oceanography*, *19*(4), pp.551-560.

Baumann, H., Doherty, O., 2013. Decadal changes in the world's coastal latitudinal temperature gradients. *PloS one*, *8*(6), p.e67596

Beaufort, L., de Garidel-Thoron, T., Mix, A.C., Pisias, N.G., 2001. ENSO-like forcing on oceanic primary production during the late Pleistocene. *Science*, *293*(5539), pp.2440-2444.

Belkin, I.M., 2009. Rapid warming of large marine ecosystems. *Progress in Oceanography*, *81*(1-4), pp.207-213.

Biller, D. V., Coale, T. H., Till, R. C., Smith, G. J., & Bruland, K. W. (2013). Coastal iron and nitrate distributions during the spring and summer upwelling season in the central California Current upwelling regime. *Continental Shelf Research*, *66*, 58-72.

Bjerknes, J., 1969. Atmospheric teleconnections from the equatorial Pacific. *Mon. Wea. Rev*, *97*(3), pp.163-172.

Blanco, J.L., Thomas, A.C., Carr, M.E., Strub, P.T., 2001. Seasonal climatology of hydrographic conditions in the upwelling region off northern Chile. *Journal of Geophysical Research: Oceans*, *106*(C6), pp.11451-11467.

Blanchette, M.L., Pearson, R.G., 2012. Macroinvertebrate assemblages in rivers of the Australian dry tropics are highly variable. *Freshwater Science*, *31*(3), pp.865-881.

Blamey, L.K., Howard, J.A., Agenbag, J., Jarre, A., 2012. Regime-shifts in the southern Benguela shelf and inshore region. *Progress in Oceanography*, *106*, pp.80-95.

Bograd, S.J., Schroeder, I., Sarkar, N., Qiu, X., Sydeman, W.J. and Schwing, F.B., 2009. Phenology of coastal upwelling in the California Current. *Geophysical Research Letters*, *36*(1).

Borges, M.F., Santos, A.M.P., Crato, N., Mendes, H., Mota, B., 2003. Sardine regime shifts off Portugal: a time series analysis of catches and wind conditions. *Scientia Marina*, *67*(S1), pp.235-244.

Boyd, A.J., Salat, J., Masó, M., 1987. The seasonal intrusion of relatively saline water on the shelf off northern and central Namibia. *South African Journal of Marine Science*, *5*(1), pp.107-120.

Boyer, D.C., Hampton, I., 2001. An overview of the living marine resources of Namibia. *African Journal of Marine Science*, *23*, pp.5-35.

Brasnett, B., 2008. The impact of satellite retrievals in a global sea-surface-temperature analysis. *Quarterly Journal of the Royal Meteorological Society*, *134*(636), pp.1745-1760.

Brady, R.X., Alexander, M.A., Lovenduski, N.S., Rykaczewski, R.R., 2017. Emergent anthropogenic trends in California Current upwelling. *Geophysical Research Letters*, *44*(10), pp.5044-5052.

Brady, R.X., Lovenduski, N.S., Alexander, M.A., Jacox, M. and Gruber, N., 2019. On the role of climate modes in modulating the air–sea CO2 fluxes in eastern boundary upwelling systems. *Biogeosciences*, *16*(2), pp.329-346.

Broitman, B.R., Mieszkowska, N., Helmuth, B. and Blanchette, C.A., 2008. Climate and recruitment of rocky shore intertidal invertebrates in the eastern North Atlantic. *Ecology*, *89*(sp11), pp.S81-S90.

Brown, O. B., Brown, J. W., Evans, R. H., 1985. Calibration of advanced very high resolution radiometer infrared observations. *Journal of Geophysical Research: Oceans*, *90*(C6), pp.11667-11677.

Bulgin, C.E., Embury, O., Merchant, C. J., 2016. Sampling uncertainty in gridded sea surface temperature products and Advanced Very High Resolution Radiometer (AVHRR) Global Area Coverage (GAC) data. *Remote Sensing of Environment*, *177*, pp.287-294.

Capet, X.J., Marchesiello, P., McWilliams, J.C., 2004. Upwelling response to coastal wind profiles. *Geophysical Research Letters*, *31*(13).

Cardone, V.J., Greenwood, J.G, Cane, M.A., 1990. "On trends in historical marine wind data." *Journal of Climate*, PP.113-127.

Carr, M.E., 2001. Estimation of potential productivity in Eastern Boundary Currents using remote sensing. *Deep Sea Research Part II: Topical Studies in Oceanography*, *49*(1-3), pp.59-80.

Carr, M.E., Kearns, E.J., 2003. Production regimes in four Eastern Boundary Current systems. *Deep Sea Research Part II: Topical Studies in Oceanography*, *50*(22-26), pp.3199-3221.

Casabella, N., Lorenzo, M.N., Taboada, J.J., 2014. Trends of the Galician upwelling in the context of climate change. *Journal of Sea Research*, *93*, pp.23-27.

Chao, Y., Li, Z., Farrara, J. D., Hung, P. (2009). Blending sea surface temperatures from multiple satellites and in situ observations for coastal oceans. *Journal of Atmospheric and Oceanic Technology*, *26*(7), pp.1415-1426.

Chaigneau, A., Eldin, G., Dewitte, B., 2009. Eddy activity in the four major upwelling systems from satellite altimetry (1992–2007). *Progress in Oceanography*, *83*(1-4), pp.117-123.

Chavez, F.P., Messié, M., 2009. A comparison of eastern boundary upwelling ecosystems. *Progress in Oceanography*, *83*(1-4), pp.80-96.

Chhak, K., Di Lorenzo, E., 2007. Decadal variations in the California Current upwelling cells. *Geophysical Research Letters*, *34*(14).

Cury, P. and Roy, C., 1989. Optimal environmental window and pelagic fish recruitment success in upwelling areas. *Canadian Journal of Fisheries and Aquatic Sciences*, *46*(4), pp.670-680.

Cole, D., 1999. *Franz Boas: the early years, 1859-1906*. Douglas & McIntyre.

Cowtan, K., Rohde, R., Hausfather, Z., 2018. Evaluating biases in sea surface temperature records using coastal weather stations. *Quarterly Journal of the Royal Meteorological Society*, *144*(712), pp.670-681.

Cury, P. and Shannon, L., 2004. Regime shifts in upwelling ecosystems: observed changes and possible mechanisms in the northern and southern Benguela. *Progress in Oceanography*, *60*(2-4), pp.223-243.

Dewitte, B., Vazquez-Cuervo, J., Goubanova, K., Illig, S., Takahashi, K., Cambon, G., Purca, S., Correa, D., Gutiérrez, D., Sifeddine, A., Ortlieb, L., 2012. Change in El Nino flavours over 1958–2008: Implications for the long-term trend of the upwelling off Peru. *Deep Sea Research Part II: Topical Studies in Oceanography*, *77*, pp.143-156.

Diaz, H.F., Hoerling, M.P. and Eischeid, J.K., 2001. ENSO variability, teleconnections and climate change. *International Journal of Climatology: A Journal of the Royal Meteorological Society*, *21*(15), pp.1845-1862.

Diffenbaugh, N.S., Snyder, M.A., Sloan, L.C., 2004. Could CO2-induced land-cover feedbacks alter near-shore upwelling regimes?. *Proceedings of the National Academy of Sciences*, *101*(1), pp.27-32.

Di Lorenzo, E., Schneider, N., Cobb, K.M., Franks, P.J.S., Chhak, K., Miller, A.J., McWilliams, J.C., Bograd, S.J., Arango, H., Curchitser, E., Powell, T.M., 2008. North Pacific Gyre Oscillation links ocean climate and ecosystem change. *Geophysical Research Letters*, *35*(8).

Doney, S.C., Ruckelshaus, M., Duffy, J.E., Barry, J.P., Chan, F., English, C.A., Galindo, H.M., Grebmeier, J.M., Hollowed, A.B., Knowlton, N., Polovina, J., 2011. Climate change impacts on marine ecosystems.

Dong, B., Sutton, R.T., Scaife, A.A., 2006. Multidecadal modulation of El Niño–Southern Oscillation (ENSO) variance by Atlantic Ocean sea surface temperatures. *Geophysical Research Letters*, *33*(8).

Donlon, C. J., Martin, M., Stark, J., Roberts-Jones, J., Fiedler, E., Wimmer, W., 2012. The operational sea surface temperature and sea ice analysis (OSTIA) system. *Remote Sensing of Environment*, *116*, pp.140-158.

Dorman, C.E., Winant, C.D., 2000. The structure and variability of the marine atmosphere around the Santa Barbara Channel. *Monthly Weather Review*, *128*(2), pp.261-282.

Dufois, F., Penven, P., Whittle, C.P., Veitch, J., 2012. On the warm nearshore bias in Pathfinder monthly SST products over Eastern Boundary Upwelling Systems. *Ocean Modelling*, *47*, pp.113-118.

Echevin, V., Albert, A., Lévy, M., Graco, M., Aumont, O., Piétri, A., Garric, G., 2014. Intraseasonal variability of nearshore productivity in the Northern Humboldt Current System: The role of coastal trapped waves. *Continental Shelf Research*, *73*, pp.14-30.

Escribano, R., Daneri, G., Farías, L., Gallardo, V.A., González, H.E., Gutiérrez, D., Lange, C.B., Morales, C.E., Pizarro, O., Ulloa, O., Braun, M., 2004. Biological and chemical consequences of the 1997–1998 El Niño in the Chilean coastal upwelling system: a synthesis. *Deep Sea Research Part II: Topical Studies in Oceanography*, *51*(20-21), pp.2389-2411.

Espinoza-Morriberón, D., Echevin, V., Colas, F., Tam, J., Ledesma, J., Vásquez, L., Graco, M., 2017. Impacts of E l N iño events on the P eruvian upwelling system productivity. *Journal of Geophysical Research: Oceans*, *122*(7), pp.5423-5444.

Fennel, W., 1999. Theory of the Benguela upwelling system. *Journal of Physical Oceanography*, *29*(2), pp.177-190.

Fielding, P. J., Davis, C. L., 1989. Carbon and nitrogen resources available to kelp bed filter feeders in an upwelling environment. *Marine Ecology Progress Series*, pp.181-189.

Florenchie, P., Reason, C.J.C., Lutjeharms, J.R.E., Rouault, M., Roy, C., Masson, S., 2004. Evolution of interannual warm and cold events in the southeast Atlantic Ocean. *Journal of Climate*, *17*(12), pp.2318-2334.

Fogt, R.L. and Bromwich, D.H., 2006. Decadal variability of the ENSO teleconnection to the high-latitude South Pacific governed by coupling with the southern annular mode. *Journal of Climate*, *19*(6), pp.979-997.

Fréon, P., Arístegui, J., Bertrand, A., Crawford, R.J., Field, J.C., Gibbons, M.J., Tam, J., Hutchings, L., Masski, H., Mullon, C., Ramdani, M., 2009. Functional group biodiversity in Eastern Boundary Upwelling Ecosystems questions the wasp-waist trophic structure. *Progress in Oceanography*, *83*(1-4), pp.97-106.

Finkelstein, P.L., 1981. "Measuring the dynamic performance of wind vanes." *Journal of Applied Meteorology* 20, no. 5: 588-594.

García-Reyes, M., Largier, J., 2010. Observations of increased wind-driven coastal upwelling off central California. *Journal of Geophysical Research: Oceans*, *115*(C4).

García-Reyes, M., Sydeman, W.J., Schoeman, D.S., Rykaczewski, R.R., Black, B.A., Smit, A.J., Bograd, S.J., 2015. Under pressure: climate change, upwelling, and eastern boundary upwelling ecosystems. *Frontiers in Marine Science*, *2*, p.109.

Garreaud, R.D., Falvey, M., 2009. The coastal winds off western subtropical South America in future climate scenarios. *International Journal of Climatology: A Journal of the Royal Meteorological Society*, *29*(4), pp.543-554.

Gillett, N.P., Fyfe, J.C., Parker, D.E., 2013. Attribution of observed sea level pressure trends to greenhouse gas, aerosol, and ozone changes. *Geophysical Research Letters*, *40*(10), pp.2302-2306.

Graco, M.I., Purca, S., Dewitte, B., Castro, C.G., Morón, O., Ledesma, J., Flores, G., Gutiérrez, D., 2017. The OMZ and nutrient features as a signature of interannual and low-frequency variability in the Peruvian upwelling system.

Grise, K.M., Davis, S.M., Simpson, I.R., Waugh, D.W., Fu, Q., Allen, R.J., Rosenlof, K.H., Ummenhofer, C.C., Karnauskas, K.B., Maycock, A.C. and Quan, X.W., 2019. Recent tropical expansion: Natural variability or forced response?. *Journal of Climate*, *32*(5), pp.1551-1571.

Grise, K.M. and Davis, S.M., 2020. Hadley cell expansion in CMIP6 models. *Atmospheric Chemistry & Physics*, *20*(9).

Guastella, L.A., 1992. Sea surface heat exchange at St Helena Bay and implications for the southern Benguela upwelling system. *South African Journal of Marine Science*, 12(1), pp.61-70.

Gruber, N., Lachkar, Z., Frenzel, H., Marchesiello, P., Münnich, M., McWilliams, J.C., Nagai, T., Plattner, G.K., 2011. Eddy-induced reduction of biological production in eastern boundary upwelling systems. *Nature geoscience*, *4*(11), pp.787-792.

Guastella, L.A., 1992. Sea surface heat exchange at St Helena Bay and implications for the southern Benguela upwelling system. *South African Journal of Marine Science*, *12*(1), pp.61-70.

Gutknecht, E., Dadou, I., Marchesiello, P., Cambon, G., Le Vu, B., Sudre, J., Garçon, V., Machu, E., Rixen, T., Kock, A., Flohr, A., 2013. Nitrogen transfers off Walvis Bay: a 3-D coupled physical/biogeochemical modeling approach in the Namibian upwelling system. *Biogeosciences*, *10*(6), pp.4117-4135.

Haack, T., Chelton, D., Pullen, J., Doyle, J.D., Schlax, M., 2008. Summertime influence of SST on surface wind stress off the US West Coast from the US Navy COAMPS model. *Journal of physical oceanography*, *38*(11), pp.2414-2437.

Hagen, E., 2009. Atlantic Exploration and Climate. *Selected Contributions on Results of Climate Research in East Germany*, pp.80-95.

Hall, D.K., Comiso, J.C., DiGirolamo, N.E., Shuman, C.A., Key, J.R. and Koenig, L.S., 2012. A satellite-derived climate-quality data record of the clear-sky surface temperature of the Greenland ice sheet. *Journal of Climate*, *25*(14), pp.4785-4798.

Halpern, D., 2002. Offshore Ekman transport and Ekman pumping off Peru during the 1997–1998 El Nino. *Geophysical Research Letters*, *29*(5), pp.19-1.

Harlass, J., Latif, M., Park, W., 2015. Improving climate model simulation of tropical Atlantic sea surface temperature: The importance of enhanced vertical atmosphere model resolution. *Geophysical Research Letters*, *42*(7), pp.2401-2408.

Harley, C.D., Randall Hughes, A., Hultgren, K.M., Miner, B.G., Sorte, C.J., Thornber, C.S., Rodriguez, L.F., Tomanek, L., Williams, S.L., 2006. The impacts of climate change in coastal marine systems. *Ecology letters*, *9*(2), pp.228-241.

Hausfather, Z., Cowtan, K., Menne, M.J., Williams Jr, C.N., 2016. Evaluating the impact of US historical climatology network homogenization using the US climate reference network. *Geophysical Research Letters*, *43*(4), pp.1695-1701.

Hoegh-Guldberg, O., Bruno, J.F., 2010. The impact of climate change on the world's marine ecosystems. *Science*, *328*(5985), pp.1523-1528.

Holbrook, N.J., Goodwin, I.D., McGregor, S., Molina, E. and Power, S.B., 2011. ENSO to multi-decadal time scale changes in East Australian Current transports and Fort Denison sea level: Oceanic Rossby waves as the connecting mechanism. *Deep Sea Research Part II: Topical Studies in Oceanography*, *58*(5), pp.547-558.

Hutchings, L., Van der Lingen, C. D., Shannon, L. J., Crawford, R. J. M., Verheye, H. M. S., Bartholomae, C. H., Van der Plas, A. K., Louw, D., Kreiner, A., Ostrowski, M., Fidel, Q., 2009. The Benguela Current: An ecosystem of four components. *Progress in Oceanography*, *83*(1-4), pp.15-32.

Huyer, A., 1983. Coastal upwelling in the California Current system. *Progress in oceanography*, *12*(3), pp.259-284.

Hsieh, W.W., Boer, G.J., 1992. Global climate change and ocean upwelling. *Fisheries Oceanography*, *1*(4), pp.333-338.

Jacox, M.G., Fiechter, J., Moore, A.M., Edwards, C.A., 2015. ENSO and the C alifornia C urrent coastal upwelling response. *Journal of Geophysical Research: Oceans*, *120*(3), pp.1691-1702.

Jakoboski, J., Todd, R.E., Owens, W.B., Karnauskas, K.B., Rudnick, D.L., 2020. Bifurcation and upwelling of the equatorial undercurrent west of the Galapagos archipelago. *Journal of Physical Oceanography*, *50*(4), pp.887-905.

Jury, M.R., 1980. Characteristics of summer wind field and air sea interaction over the Cape Peninsula upwelling regions. M.Sc. Thesis. University of Cape Town, South Africa.

Kennedy, J.J., Rayner, N.A., Smith, R.O., Parker, D.E., Saunby, M., 2011. Reassessing biases and other uncertainties in sea surface temperature observations measured in situ since 1850: 1. Measurement and sampling uncertainties. *Journal of Geophysical Research: Atmospheres*, *116*(D14).

Kessler, W.S., 2002. Is ENSO a cycle or a series of events?. *Geophysical Research Letters*, *29*(23), pp.40-1.

Kilpatrick, K.A., Podesta, G.P., Evans, R., 2001. Overview of the NOAA/NASA advanced very high resolution radiometer Pathfinder algorithm for sea surface temperature and associated matchup database. *Journal of Geophysical Research: Oceans*, *106*(C5), pp.9179-9197.

Klein, S.A., Soden, B.J., Lau, N.C., 1999. Remote sea surface temperature variations during ENSO: Evidence for a tropical atmospheric bridge. *Journal of climate*, *12*(4), pp.917-932.

Lau, N.C., 1997. Interactions between global SST anomalies and the midlatitude atmospheric circulation. *Bulletin of the American Meteorological Society*, *78*(1), pp.21-34.

Levitus, Sydney, John I. Antonov, Julian Wang, Thomas L. Delworth, Keith W. Dixon, and Anthony J. Broccoli. "Anthropogenic warming of Earth's climate system." *Science* 292, no. 5515 (2001): 267-270.

Liu, Y. and Minnett, P.J., 2016. Sampling errors in satellite-derived infrared sea-surface temperatures. Part I: Global and regional MODIS fields. *Remote sensing of environment*, *177*, pp.48-64.

Lima, F.P., Wethey, D.S., 2012. Three decades of high-resolution coastal sea surface temperatures reveal more than warming. *Nature communications*, *3*(1), pp.1-13.

Lu, F., Hu, H., Sun, W., Zhu, J., Liu, G., Zhou, W., Zhang, Q., Shi, P., Liu, X., Wu, X., Zhang, L., 2018. Effects of national ecological restoration projects on carbon sequestration in China from 2001 to 2010. *Proceedings of the National Academy of Sciences*, *115*(16), pp.4039-4044.

McGregor, H.V., Dima, M., Fischer, H.W. and Mulitza, S., 2007. Rapid 20th-century increase in coastal upwelling off northwest Africa. *science*, *315*(5812), pp.637-639.

Mead, A., Griffiths, C.L., Branch, G.M., McQuaid, C.D., Blamey, L.K., Bolton, J.J., Anderson, R.J., Dufois, F., Rouault, M., Froneman, P.W., Whitfield, A.K., 2013. Human-mediated drivers of change—impacts on coastal ecosystems and marine biota of South Africa. *African Journal of Marine Science*, *35*(3), pp.403-425.

Menne, M.J., Williams Jr, C.N., Vose, R.S., 2009. The US Historical Climatology Network monthly temperature data, version 2. *Bulletin of the American Meteorological Society*, *90*(7), pp.993-1008.

Mesias, J.M., Bisagni, J.J. and Brunner, A.M., 2007. A high-resolution satellite-derived sea surface temperature climatology for the western North Atlantic Ocean. *Continental Shelf Research*, *27*(2), pp.191-207.

Messié, M., Ledesma, J., Kolber, D.D., Michisaki, R.P., Foley, D.G., Chavez, F.P., 2009. Potential new production estimates in four eastern boundary upwelling ecosystems. *Progress in Oceanography*, *83*(1-4), pp.151-158.

Minnett, P.J., 1991. Consequences of sea surface temperature variability on the validation and applications of satellite measurements. *Journal of Geophysical Research: Oceans*, *96*(C10), pp.18475-18489.

Minnett, P.J., Brown, O.B., Evans, R.H., Key, E.L., Kearns, E.J., Kilpatrick, K., Kumar, A., Maillet, K.A. and Szczodrak, G., 2004, September. Sea-surface temperature measurements from the Moderate-Resolution Imaging Spectroradiometer (MODIS) on Aqua and Terra. In *IGARSS 2004. 2004 IEEE International Geoscience and Remote Sensing Symposium* (Vol. 7, pp. 4576-4579). Ieee.

Morales, C.E., Hormazábal, S.E., Blanco, J., 1999. Interannual variability in the mesoscale distribution of the depth of the upper boundary of the oxygen minimum layer off northern Chile (18–24S): Implications for the pelagic system and biogeochemical cycling. *Journal of Marine Research*, 57(6), pp.909-932.

Montecino, V., Rutllant, J., Salinas, S., 2005. Coastal ocean circulation off western South America. *The Global Coastal Ocean-Regional Studies and Syntheses*, *11*, p.273.

Montecino, V., Lange, C.B., 2009. The Humboldt Current System: Ecosystem components and processes, fisheries, and sediment studies. *Progress in Oceanography*, *83*(1-4), pp.65-79.

Morgan, C. A., Peterson, W. T., & Emmett, R. L. (2003). Onshore offshore variations in copepod community structure off the Oregon coast during the summer upwelling season. *Marine Ecology Progress Series*, *249*, 223-236.

Morales, C.E., Hormazábal, S.E., Blanco, J., 1999. Interannual variability in the mesoscale distribution of the depth of the upper boundary of the oxygen minimum layer off northern Chile (18–24S): Implications for the pelagic system and biogeochemical cycling. *Journal of Marine Research*, *57*(6), pp.909-932.

Mote, P.W., Mantua, N.J., 2002. Coastal upwelling in a warmer future. *Geophysical research letters*, *29*(23), pp.53-1.

Mote, P.W., Salathé, E.P., 2010. Future climate in the Pacific Northwest. *Climatic change*, *102*(1-2), pp.29-50.

Murawski, S.A., 1993. Climate change and marine fish distributions: forecasting from historical analogy. *Transactions of the American Fisheries Society*, *122*(5), pp.647-658.

Narayan, N., 2010. Interactive comment on "Trends in coastal upwelling intensity during the late 20th century" by N. Narayan et al.

Nelson, G., Hutchings, L., 1983. The Benguela upwelling area. *Progress in Oceanography*, *12*(3), pp.333-356.

Pardo, P.C., Padín, X.A., Gilcoto, M., Farina-Busto, L., Pérez, F.F., 2011. Evolution of upwelling systems coupled to the long-term variability in sea surface temperature and Ekman transport. *Climate Research*, *48*(2-3), pp.231-246.

Parker, D.E., Folland, C.K., Jackson, M., 1995. Marine surface temperature: observed variations and data requirements. *Climatic Change*, *31*(2-4), pp.559-600.

Pauly, D., Christensen, V., 1995. Primary production required to sustain global fisheries. *Nature*, 374(6519), pp.255-257.

Pegliasco, C., Chaigneau, A., Morrow, R., 2015. Main eddy vertical structures observed in the four major Eastern Boundary Upwelling Systems. *Journal of Geophysical Research: Oceans*, *120*(9), pp.6008-6033.

Phillips, N. E. (2005). Growth of filter-feeding benthic invertebrates from a region with variable upwelling intensity. *Marine Ecology Progress Series*, *295*, 79-89.

Pelegrí, J.L., Peña-Izquierdo, J., 2015. Inorganic nutrients and dissolved oxygen in the Canary Current Large Marine Ecosystem.

Peterson, W.T., Schwing, F.B., 2003. A new climate regime in northeast Pacific ecosystems. *Geophysical research letters*, *30*(17).

Perlin, N., Samelson, R.M., Chelton, D.B., 2004. Scatterometer and model wind and wind stress in the Oregon–northern California coastal zone. *Monthly Weather Review*, *132*(8), pp.2110-2129.

Perlin, N., Skyllingstad, E.D., Samelson, R.M., 2010. Coastal Atmospheric Circulation around a Cape and its Response to Wind-Driven Upwelling Studied Using a Coupled Ocean-Atmosphere Model.

Perlin, N., Skyllingstad, E.D., Samelson, R.M., 2011. Coastal atmospheric circulation around an idealized cape during wind-driven upwelling studied from a coupled ocean–atmosphere model. *Monthly Weather Review*, *139*(3), pp.809-829.

Rahmstorf, S., 2002. Ocean circulation and climate during the past 120,000 years. *Nature*, *419*(6903), pp.207-214.

Rasmusson, E.M., Carpenter, T.H., 1982. Variations in tropical sea surface temperature and surface wind fields associated with the Southern Oscillation/El Niño. *Monthly Weather Review*, *110*(5), pp.354-384.

Rayner, N.A., Brohan, P., Parker, D.E., Folland, C.K., Kennedy, J.J., Vanicek, M., Ansell, T.J. and Tett, S.F.B., 2006. Improved analyses of changes and uncertainties in sea surface temperature measured in situ since the mid-nineteenth century: The HadSST2 dataset. *Journal of Climate*, *19*(3), pp.446-469.

Reynolds, R.W., Smith, T.M., 1994. Improved global sea surface temperature analyses using optimum interpolation. *Journal of climate*, *7*(6), pp.929-948.

Reynolds, R.W., Smith, T.M., 1995. A high-resolution global sea surface temperature climatology. *Journal of Climate*, *8*(6), pp.1571-1583.

Reynolds, R.W., Rayner, N.A., Smith, T.M., Stokes, D.C., Wang, W., 2002. An improved in situ and satellite SST analysis for climate. *Journal of climate*, *15*(13), pp.1609-1625.

Reynolds, R.W., Chelton, D.B., 2010. Comparisons of daily sea surface temperature analyses for 2007–08. *Journal of climate*, *23*(13), pp.3545-3562.

Reynolds, R.W., Chelton, D.B., Roberts-Jones, J., Martin, M.J., Menemenlis, D., Merchant, C.J., 2013. Objective determination of feature resolution in two sea surface temperature analyses. *Journal of climate*, *26*(8), pp.2514-2533.

Ricciardulli, L., Wentz, F.J., 2004. Uncertainties in sea surface temperature retrievals from space: Comparison of microwave and infrared observations from TRMM. *Journal of Geophysical Research: Oceans*, *109*(C12).

Rimbu, N., Lohmann, G., Kim, J.H., Arz, H.W., Schneider, R., 2003. Arctic/North Atlantic Oscillation signature in Holocene sea surface temperature trends as obtained from alkenone data. *Geophysical research letters*, *30*(6).

Risien, C.M., Reason, C.J.C., Shillington, F.A., Chelton, D.B., 2004. Variability in satellite winds over the Benguela upwelling system during 1999–2000. *Journal of Geophysical Research: Oceans*, *109*(C3).

Robertson, A. W., Mechoso, C. R., & Kim, Y. J. (2000). The influence of Atlantic sea surface temperature anomalies on the North Atlantic Oscillation. *Journal of Climate*, *13*(1), 122-138.

Robinson, I. S., Wells, N. C. and Charnock, H. (1984). The sea surface thermal boundary layer and its relevance to the measurement of sea surface temperature by airborne and spaceborne radiometers. *International Journal of Remote Sensing*, *5*(1), pp.19-45.

Rollo, C., Heywood, K. J., Hall, R. A., Barton, E. D., & Kaiser, J. (2020). Glider observations of the Northwestern Iberian margin during an exceptional summer upwelling season. *Journal of Geophysical Research: Oceans*, *125*(8), e2019JC015804.

Roemmich, D., McGowan, J., 1995. Climatic warming and the decline of zooplankton in the California Current. *Science*, *267*(5202), pp.1324-1326.

Rossi, V., 2010. *Influence of mesoscale physical processes on planktonic ecosystems in the regional ocean: application to the Eastern Boundary Upwelling Systems* (Doctoral dissertation). *Science of the Universe [Physics]/Ocean, Atmosphere*.

Rouault, M., Florenchie, P., Fauchereau, N., Reason, C.J., 2003. South East tropical Atlantic warm events and southern African rainfall. *Geophysical Research Letters*, *30*(5).

Rouault, M., Pohl, B., Penven, P., 2010. Coastal oceanic climate change and variability from 1982 to 2009 around South Africa. *African Journal of Marine Science*, *32*(2), pp.237-246.

Rykaczewski, R.R., Dunne, J.P., Sydeman, W.J., García-Reyes, M., Black, B.A., Bograd, S.J., 2015. Poleward displacement of coastal upwelling-favorable winds in the ocean's eastern boundary currents through the 21st century. *Geophysical Research Letters*, *42*(15), pp.6424-6431.

Saji, N.H., Goswami, B.N., Vinayachandran, P.N. and Yamagata, T., 1999. A dipole mode in the tropical Indian Ocean. *Nature*, *401*(6751), pp.360-363.

Samanta, D., Karnauskas, K.B., Goodkin, N.F., 2019. Tropical Pacific SST and ITCZ biases in climate models: Double trouble for future rainfall projections?. *Geophysical Research Letters*, *46*(4), pp.2242-2252.

Santos, F., Gomez-Gesteira, M., Decastro, M., Alvarez, I., 2012. Differences in coastal and oceanic SST trends due to the strengthening of coastal upwelling along the Benguela current system. *Continental Shelf Research*, *34*, pp.79-86.

Seabra, R., Varela, R., Santos, A.M., Gómez-Gesteira, M., Meneghesso, C., Wethey, D.S., Lima, F.P., 2019. Reduced nearshore warming associated with eastern boundary upwelling systems. *Frontiers in Marine Science*, *6*, p.104.

Schlegel, R.W., Smit, A.J., 2016. Climate change in coastal waters: time series properties affecting trend estimation. *Journal of Climate*, *29*(24), pp.9113-9124.

Schlegel, R.W., Oliver, E.C., Perkins-Kirkpatrick, S., Kruger, A., Smit, A.J., 2017. Predominant atmospheric and oceanic patterns during coastal marine heatwaves. *Frontiers in Marine Science*, *4*, p.323.

Schlegel, R.W., Smit, A.J., 2018. heatwaveR: a central algorithm for the detection of heatwaves and cold-spells. *Journal of Open Source Software*, *3*(27), p.821.

Schultz, O.J., 2010. *Belonging to the West Coast: an ethnography of St Helena Bay in the context of marine resource scarcity* (Doctoral dissertation, University of Cape Town).

Scoccimarro, E., Gualdi, S., Bellucci, A., Sanna, A., Giuseppe Fogli, P., Manzini, E., Vichi, M., Oddo, P., Navarra, A., 2011. Effects of tropical cyclones on ocean heat transport in a high-resolution coupled general circulation model. *Journal of Climate*, *24*(16), pp.4368-4384.

Servain, J., Picaut, J., Busalacchi, A.J., 1985. Interannual and seasonal variability of the tropical Atlantic Ocean depicted by sixteen years of sea-surface temperature and wind stress. In *Elsevier oceanography series* (Vol. 40, pp. 211-237). Elsevier.

Shaffer, G., Pizarro, O., Djurfeldt, L., Salinas, S., Rutllant, J., 1997. Circulation and low-frequency variability near the Chilean coast: Remotely forced fluctuations during the 1991–92 El Nino. *Journal of Physical Oceanography*, *27*(2), pp.217-235.

Shannon, L.V., 1985. The Benguela ecosystem. I: Evolution of the Benguela physical features and processes. Oceanography and Marine Biology, 23, pp.105-182.

Shannon, L.V., Boyd, A.J., Brundrit, G.B., Taunton-Clark, J., 1986. On the existence of an El Niño-type phenomenon in the Benguela system. *Journal of marine Research*, *44*(3), pp.495-520.

Smith, T.M., Reynolds, R.W., 1998. A high-resolution global sea surface temperature climatology for the 1961–90 base period. *Journal of Climate*, *11*(12), pp.3320-3323.

Smit, A.J., Roberts, M., Anderson, R.J., Dufois, F., Dudley, S.F., Bornman, T.G., Olbers, J., Bolton, J.J., 2013. A coastal seawater temperature dataset for biogeographical studies: large biases between in situ and remotely-sensed data sets around the coast of South Africa. *PLoS One*, *8*(12).

Snyder, M.A., Sloan, L.C., Diffenbaugh, N.S., Bell, J.L., 2003. Future climate change and upwelling in the California Current. *Geophysical Research Letters*, *30*(15).

Sohn, B.J., Yeh, S.W., Schmetz, J. and Song, H.J., 2013. Observational evidences of Walker circulation change over the last 30 years contrasting with GCM results. *Climate Dynamics*, *40*(7-8), pp.1721-1732.

Stenseth, N.C., Mysterud, A., Ottersen, G., Hurrell, J.W., Chan, K.S., Lima, M., 2002. Ecological effects of climate fluctuations. *Science*, *297*(5585), pp.1292-1296.

Stander, G.H., De Decker, A.H.B., 1969. *Some physical and biological aspects of an oceanographic anomaly off South West Africa in 1963*. Department of Commerce, Division of Fisheries.

Stocker, T.F., Qin, D., Plattner, G.K., Tignor, M., Allen, S.K., Boschung, J., Nauels, A., Xia, Y., Bex, V., Midgley, P.M., 2013. Climate change 2013: The physical science basis. *Contribution of working group I to the fifth assessment report of the intergovernmental panel on climate change*, *1535*.

Sutton, R.T., Jewson, S.P., Rowell, D.P., 2000. The elements of climate variability in the tropical Atlantic region. *Journal of Climate*, *13*(18), pp.3261-3284.

Sydeman, W.J., Santora, J.A., Thompson, S.A., Marinovic, B., Lorenzo, E.D., 2013. Increasing variance in North Pacific climate relates to unprecedented ecosystem variability off California. *Global Change Biology*, *19*(6), pp.1662-1675.

Sydeman, W.J., García-Reyes, M., Schoeman, D.S., Rykaczewski, R.R., Thompson, S.A., Black, B.A., Bograd, S.J., 2014. Climate change and wind intensification in coastal upwelling ecosystems. *Science*, *345*(6192), pp.77-80.

Sverdrup, H.U., Allen, W.E., 1939. Distribution of diatoms in relation to the character of water masses and currents off southern California in 1938. *J. mar. Res*, *2*(2), pp.131-144.

Tang, D., Dana, R.K., Zhaoding, W., Jiansheng, L., Hiroshi, K., 2003. "AVHRR satellite remote sensing and shipboard measurements of the thermal plume from the Daya Bay, nuclear power station, China." *Remote Sensing of Environment* 84, no. 4: 506-515.

Tim, N., Zorita, E., Hünicke, B., 2015. Decadal variability and trends of the Benguela upwelling system as simulated in a high-resolution ocean simulation. *Ocean Science*, *11*(3), pp.483-502.

Timmermann, A., Oberhuber, J., Bacher, A., Esch, M., Latif, M., Roeckner, E., 1999. Increased El Niño frequency in a climate model forced by future greenhouse warming. *Nature*, *398*(6729), pp.694-697.

Tittensor, D.P., Mora, C., Jetz, W., Lotze, H.K., Ricard, D., Berghe, E.V., Worm, B., 2010. Global patterns and predictors of marine biodiversity across taxa. *Nature*, *466*(7310), pp.1098-1101.

Tyson, P.D., Preston-Whyte, R.A., 2000. *Weather and climate of southern Africa*. Oxford University Press.

Ulloa, O., Escribano, R., Hormazabal, S., Quinones, R.A., González, R.R., Ramos, M., 2001. Evolution and biological effects of the 1997–98 El Nino in the upwelling ecosystem off northern Chile. *Geophysical Research Letters*, *28*(8), pp.1591-1594.

Vallis, G.K., 1986. El Niño: A chaotic dynamical system?. *Science*, *232*(4747), pp.243-245.

Van Heerden, J., Hurry, L., 1998. Southern Africa's weather patterns: An introductory guide. Collegium.

Varela, R., Álvarez, I., Santos, F., DeCastro, M., & Gómez-Gesteira, M. (2015). Has upwelling strengthened along worldwide coasts over 1982-2010?. *Scientific reports*, *5*(1), 1-15.

Vargas, G., Pantoja, S., Rutllant, J.A., Lange, C.B., Ortlieb, L., 2007. Enhancement of coastal upwelling and interdecadal ENSO-like variability in the Peru-Chile Current since late 19th century. *Geophysical Research Letters*, *34*(13).

Walker, A., 2020. *Observed Trends of Coastal Upwelling in Eastern Boundary Upwelling Systems* (Doctoral dissertation, University of Colorado at Boulder).

Wang, W., McPhaden, M.J., 2000. The surface-layer heat balance in the equatorial Pacific Ocean. Part II: Interannual variability. *Journal of Physical Oceanography*, *30*(11), pp.2989-3008.

Wang, C., 2004. ENSO, Atlantic climate variability, and the Walker and Hadley circulations. In *The Hadley circulation: Present, past and future* (pp. 173-202). Springer, Dordrecht.

Wang, X.L., Cai, X.D., Su, Z.E., Chen, M.C., Wu, D., Li, L., Liu, N.L., Lu, C.Y., Pan, J.W., 2015. Quantum teleportation of multiple degrees of freedom of a single photon. *Nature*, *518*(7540), pp.516-519.

Whitfield, A.K., James, N.C., Lamberth, S.J., Adams, J.B., Perissinotto, R., Rajkaran, A., Bornman, T.G., 2016. The role of pioneers as indicators of biogeographic range expansion caused by global change in southern African coastal waters. *Estuarine, Coastal and Shelf Science*, *172*, pp.138-153.

Wick, G.A., Emery, W.J., Schluessel, P., 1992. A comprehensive comparison between satellite-measured skin and multichannel sea surface temperature. *Journal of Geophysical Research: Oceans*, *97*(C4), pp.5569-5595.

Wycech, J.B., Gill, E., Rajagopalan, B., Marchitto Jr, T.M., Molnar, P.H., 2020. Multiproxy Reduced-Dimension Reconstruction of Pliocene Equatorial Pacific Sea Surface Temperatures. *Paleoceanography and Paleoclimatology*, *35*(1), p.e2019PA003685.

Yeh, S.W., Cai, W., Min, S.K., McPhaden, M.J., Dommenget, D., Dewitte, B., Collins, M., Ashok, K., An, S.I., Yim, B.Y. and Kug, J.S., 2018. ENSO atmospheric teleconnections and their response to greenhouse gas forcing. *Reviews of Geophysics*, *56*(1), pp.185-206.

Zebiak, S.E., 1993. Air–sea interaction in the equatorial Atlantic region. *Journal of Climate*, *6*(8), pp.1567-1586.

Zhang, L., Han, W., Karnauskas, K.B., Meehl, G.A., Hu, A., Rosenbloom, N., Shinoda, T., 2019. Indian Ocean warming trend reduces Pacific warming response to anthropogenic greenhouse gases: An interbasin thermostat mechanism. *Geophysical Research Letters*, *46*(19), pp.10882-10890.